

---

## Reaction Dynamics and Charge Transfer in the Scattering of State-Selected Ions on Surfaces

Patricia L. Maazouz

### Publication Date

15-04-2004

### License

This work is made available under a All Rights Reserved license and should only be used in accordance with that license.

### Citation for this work (American Psychological Association 7th edition)

Maazouz, P. L. (2004). *Reaction Dynamics and Charge Transfer in the Scattering of State-Selected Ions on Surfaces* (Version 1). University of Notre Dame. <https://doi.org/10.7274/7h149p30z5r>

This work was downloaded from CurateND, the University of Notre Dame's institutional repository.

For more information about this work, to report or an issue, or to preserve and share your original work, please contact the CurateND team for assistance at [curate@nd.edu](mailto:curate@nd.edu).

## APPENDICES

The optimization of the ion imaging detector was performed with Simion 3D, a computer program developed by the Idaho National Engineering Lab. The complexity of the shapes of the elements in the ion imaging detector and the critical timing between the pulsed voltages applied to each element, required the creation of the geometry file in A.1 and the simulation program in A.2. Further details for the simulations may be found in section 2.5.2.

### A.1 Flyswatter Geometry File

NSFGEOM1.gem

```
;Define Repeler
Electrode (1)
{Fill{Within{Cylinder(83,39.5,10.625,36.5,36.5,0.625)}}
  Within{Box3d(62.1,.675,10,103.9,10.675,10.625)}}}
;   Notin{Cylinder(63.625,3.25,10.625,1.5625,1.5625,0.625)}
;   Notin{Cylinder(102.375,3.25,10.625,1.5625,1.5625,0.625)}}}

;Define the bottom edges of the repeller
Locate (49.5,25,0,1,0,-63,0)
  {Electrode(1)
    {Fill{Within{Box3d(0,0,10,27.5,5,10.625)}}}}
;      Notin{Cylinder(25.75,2.5,10.625,1.5625,1.5625,0.625)}}}

Locate (104,0.5,0,1,0,63,0)
  {Electrode (1)
    {Fill{Within{Box3d(0,0,10,27.5,5,10.625)}}}}
;      Notin{Cylinder(1.75,2.5,10.625,1.5625,1.5625,0.625)}}}
;Locate (0,0,0,1,0,0,0)
;  {Electrode (1)
;    {Fill{Within{Cylinder(63.625,3.25,10.625,1.6,1.6,0.625)}}
;      Notin{Cylinder(63.625,3.25,10.625,1.5625,1.5625,0.625)}}
;      Within{Cylinder(102.375,3.25,10.625,1.6,1.6,0.625)}}}
```

```
;      Notin{Cylinder(102.375,3.25,10.625,1.5625,1.5625,0.625)}}}}
```

```
;Define the top point of the repellar
```

```
Locate (63.5,63,0,1,0,35,0)
```

```
{Electrode (1)
```

```
{Fill{Within{Box3d(0,0,10,27.5,6,10.625)}}}}
```

```
;      Notin{Cylinder(26,3.5,10.625,1.5625,1.5625,0.625)}}}}
```

```
Locate (80,79,0,1,0,-35,0)
```

```
{Electrode (1)
```

```
{Fill{Within{Box3d(0,0,10,27.5,6,10.625)}}}}
```

```
;      Notin{Cylinder(1.125,3.5,10.625,1.5625,1.5625,0.625)}}}}
```

```
Locate(0,0,0,1,0,0,0)
```

```
{Electrode(1)
```

```
{Fill{Within{Cylinder(83,80.25,10.625,1.6,1.6,0.625)}}}}
```

```
;      Notin{Cylinder(83,80.25,10.625,1.5625,1.5625,0.625)}}}}
```

```
;Define the 3 screws (0-80) and the three nuts per screw
```

```
Electrode (1)
```

```
{Fill{Within{Cylinder(83,80.25,10,1.125,1.125,1.25)}
```

```
Within{Cylinder(83,80.25,35,0.75,0.75,25)}
```

```
Within{Cylinder(83,80.25,12.875,2,2,1.125)}
```

```
Within{Cylinder(83,80.25,19.375,2,2,1.125)}
```

```
Within{Cylinder(83,80.25,25.5,2,2,1.125)}
```

```
Within{Cylinder(63.625,3.25,10,1.125,1.125,1.25)}
```

```
Within{Cylinder(63.625,3.25,35,0.75,0.75,25)}
```

```
Within{Cylinder(63.625,3.25,12.875,2,2,1.125)}
```

```
Within{Cylinder(63.625,3.25,19.375,2,2,1.125)}
```

```
Within{Cylinder(63.625,3.25,25.5,2,2,1.125)}
```

```
Within{Cylinder(102.375,3.25,10,1.125,1.125,1.25)}
```

```
Within{Cylinder(102.375,3.25,35,0.75,0.75,25)}
```

```
Within{Cylinder(102.375,3.25,12.875,2,2,1.125)}
```

```
Within{Cylinder(102.375,3.25,19.375,2,2,1.125)}
```

```
Within{Cylinder(102.375,3.25,25.5,2,2,1.125)}}}}
```

```
;Define Grounded Grid Plate
```

```
Electrode (2)
```

```
{Fill{Within{Cylinder(83,39.5,22.375,36.5,36.5,1.75)}
```

```
Notin{Cylinder(83,39.5,22.375,26.5,26.5,1.75)}
```

```
Notin{Cylinder(83,39.5,22.375,28.125,28.125,1)}
```

```
Within{Box3d(62.1,675,20.625,103.9,10.675,22.375)}}}}
```

```
;      Notin{Cylinder(63.625,3.25,22.375,1.5625,1.5625,1.75)}
```

```
;      Notin{Cylinder(102.375,3.25,22.375,1.5625,1.5625,1.75)}}}}
```

```
Locate(49.5,25,0,1,0,-63,0)
```

```
{Electrode (2)
```

```
{Fill{Within{Box3D(0,0,20.625,27.5,5,22.375)}}}}
```

```
;      Notin{Cylinder(25.75,2.5,22.375,1.5625,1.5625,1.75)}}}}
```

```

Locate(104,0.5,0,1,0,63,0)
{Electrode (2)
  {Fill{Within{box3d(0,0,20.625,27.5,5,22.375)}}}}
;    Notin{Cylinder(1.75,2.5,22.375,1.5625,1.5625,1.75)}}}}
;Locate(0,0,0,1,0,0,0)
;{Electrode(2)
;  {Fill{Within{Cylinder(63.625,3.25,22.375,1.6,1.6,1.75)}}
;    Notin{Cylinder(63.625,3.25,22.375,1.5625,1.5625,1.75)}}
;    Within{Cylinder(102.375,3.25,22.375,1.6,1.6,1.75)}}
;    Notin{Cylinder(102.375,3.25,22.375,1.5625,1.5625,1.75)}}}}

;Define the top point of the grid plate
Locate(63.5,63,0,1,0,35,0)
{Electrode (2)
  {Fill{Within{Box3d(0,0,20.625,27.5,6,22.375)}}}}
;    Notin{Cylinder(26,3.5,22.375,1.5625,1.5625,1.75)}}}}
Locate(80,79,0,1,0,-35,0)
{Electrode (2)
  {Fill{Within{Box3d(0,0,20.625,27.5,6,22.375)}}}}
;    Notin{Cylinder(1.125,3.5,22.375,1.5625,1.5625,1.75)}}}}
Locate(0,0,0,1,0,0,0)
{Electrode (2)
  {Fill{Within{Cylinder(83,80.25,22.375,1.6,1.6,1.75)}}}}
;    Notin{Cylinder(83,80.25,22.375,1.5625,1.5625,1.75)}}}}

;Define inner tube
Locate(0,0,0,1,0,0,0)
{Electrode (3)
  {Fill{Within{Cylinder(83,39.5,81.125,25,25,58.75)}}
    Notin{Cylinder(83,39.5,81.125,23.5,23.5,58.75)}}}}

;Define Outer Tube
Electrode (4)
  {Fill{Within{Cylinder(83,39.5,68.25,30,30,46.875)}}
    Notin{Cylinder(83,39.5,68.25,26.5,26.5,46.875)}}}}

;Define the outer tube holder
Electrode (4)
  {Fill{Within{Cylinder(83,39.5,68.25,37.5,37.5,1.75)}}
    Notin{Cylinder(83,39.5,68.25,26.5,26.5,1.75)}}}}

;Define the tube around the CEMA Plates
Electrode (4)
  {Fill{Within{Cylinder(83,39.5,93.25,37.5,37.5,25)}}
    Notin{Cylinder(83,39.5,93.25,32.5,32.5,25)}}}

```

```

;Define the CEMA Plate
Electrode (5)
    {Fill{Within{Cylinder(83,39.5,84.75,25,25,0.5)}}}

;Define the end of the flight tube
Electrode (4)
    {Fill{Within{Cylinder(83,39.5,93.25,37.5,37.5,1.625)}}}

;Define some points for grid 1
Electrode (3)
    {Fill{Within{Cylinder(83,39.5,81.125,23.25,23.25,0)}}}
Electrode (3)
    {Fill{Within{Cylinder(83,39.5,22.375,23.25,23.25,0)}}}
Electrode (4)
    {Fill{Within{Cylinder(83,39.5,20.0,26.5,26.5,0)}}}

;Define Deceleration Lens #4
Locate (0,0,31.25,1,90,0,0)
{Electrode (6)
    {Fill{Within{Cylinder(15.625,39.5,6.25,15.625,15.625,6.25)}}
        Notin{Cylinder(15.625,39.5,6.25,3.125,3.125,6.25)}}}
;Define Deceleration Lens #5
Locate (0,0,31.25,1,90,0,0)
{Electrode (7)
    {Fill{Within{Cylinder(15.625,39.5,34.375,15.625,15.625,25)}}
        Notin{Cylinder(15.625,39.5,34.375,5.4625,5.4625,25)}}}

;Define Deceleration Lens #6
Locate (0,0,31.25,1,90,0,0)
{Electrode (8)
    {Fill{Within{Cylinder(15.625,39.5,43.75,15.625,15.625,6.25)}}
        Notin{Cylinder(15.625,39.5,43.75,3.125,3.125,6.25)}}}
Locate (122,0,31.25,1,90,0,0)
{Electrode (9)
    {Fill{Within{Cylinder(15.625,39.5,3,5,5,3)}}}

;Define the ceramics that isolate the grid plate from the screws
;Locate(0,0,0,1,0,0,0)
;{Electrode (10)
;    {Fill{Within{Cylinder(83,80.25,24.375,2.5,2.5,5)}}
;        Notin{Cylinder(83,80.25,24.375,1.5625,1.5625,5)}}
;    {Within{Cylinder(63.625,3.25,24.375,2.5,2.5,5)}}
;        Notin{Cylinder(63.625,3.25,24.375,1.5625,1.5625,5)}}
;    {Within{Cylinder(102.375,3.25,24.375,2.5,2.5,5)}}
;        Notin{Cylinder(102.375,3.25,24.375,1.5625,1.5625,5)}}}

```

## A.2. Simion□ Simulation TOF Program

TOF-ProgramFile.txt

;Create a program that will adjust the electrode potentials  
;after a specified TOF (after leaving the surface)

;-----define the adjustable variables-----

defa Swat 3 ;swat delay in microseconds  
defa Repeller 970 ;final voltage for repeller  
defa Flight\_tube -840 ;final voltage for the flight tube  
defa rise\_time 0.02 ;rise time for swat  
defa PE\_update 0.05 ;pe surface update time step in usec

;-----define the static variables

defs first 0 ;first call flag  
defs rep\_volt\_slope 1 ;voltage ramp slope for repeller  
defs ft\_volt\_slope 1 ;voltage ramp slope for flight tube  
defs final\_ramp\_time 0 ;time at end of ramp  
defs time\_delay 0 ;time delay before starting ramp  
defs time\_excite 0 ;time at end of excite phase  
defs tmark 0 ;time for next transition  
defs color 1 ;ion color after transition  
defs next\_pe\_update 0 ;next time for pe update

;-----Start the time step adjustment-----

SEG Tstep\_adjust ;used to precisely approach both the  
;ramp start and stop transitions  
1 sto color ;assume next color is red  
rcl time\_delay  
sto tmark ;assume initial delay transition  
rcl Ion\_time\_of\_flight ;get ion's current time of flight  
x>=y goto tran2 ;if TOF is greater than tmark (swat)  
;jump to the transition subroutine  
- rcl Ion\_time\_step ;compute the time to the transition  
x<=y Exit ;if the TOF is greater than the time step exit  
x><y sto Ion\_time\_step ; else use for the time step  
exit

lbl tran2 ;test for ramp stop transition  
2 sto color ;assume next color is green  
rcl time\_excite  
sto tmark ;assume final ramp transition  
rcl Ion\_time\_of\_flight ;get ion's current time of flight  
x>=y exit ;exit if at or beyond the first transition

```

- rcl Ion_time_step           ;compute the time to the transition
x<=y exit                    ;exit if TOF is greater than the time to the transition
x>y sto Ion_time_step        ;otherwise use for the time step
exit

;-----control for the repeller and flight tube voltages---
seg Fast_Adjust
  rcl first                   ;recall the first pass flag
  x=0                         ;if this is the first time through
  gosub init                  ;setup factors first---> init

;-----check if the time is greater than the swat delay-----
  rcl time_delay              ;recall start ramp time
  rcl ion_time_of_flight      ;get ion's time of flight
  x<=y                        ;check for the end of the delay time
  goto Start_Voltages         ;if the time is less than or equal to
                              ;the swat delay then use start voltages

;-----check for end of ramp time-----
  rcl time_excite             ;recall the end of the swat delay
  rcl Ion_time_of_flight      ;get ion's time of flight
  x>y                         ;check for end of ramp time
  goto constant               ;if the time is after ramp time---->constant

;-----calculate the repeller voltage for each time step-----
  rcl Ion_time_of_flight      ;get ions flight time
  rcl time_delay -            ;calculate the time into the ramp
  rcl rep_volt_slope *        ;multiply the time by the slope to
                              ;obtain the new repeller voltage
  sto adj_elect01             ;change the repeller voltage

;-----calculate the flight tube voltage for each time step----
  rcl Ion_time_of_flight      ;get the ion's time of flight
  rcl swat -                  ;calculate the time into the ramp
  rcl ft_volt_slope *         ;obtain the new flight tube voltage
  sto adj_elect03             ;change the flight tube voltage
  exit

; -----initialize parameters for the ramp---
  lbl init
  1 sto first                 ;entry point for init routine

;-----calculate the voltage slopes---
  rcl repeller
  rcl rise_time /             ;repeller divided by the rise time
  sto rep_volt_slope          ; equals the slope for the repeller

```

```

    rcl flight_tube
    rcl rise_time /      ;flight_tube divided by the rise time
    sto ft_volt_slope    ;equals the slope for the flight tube

;-----calculate stop times for the ramp---
    rcl swat
    sto time_delay
    rcl rise_time
    + sto time_excite    ;add to the delay time and store in
                        ;time excite (end of voltage ramp)

    rtn

                        ;set repeller and flight tube to zero volts
    lbl constant         ;constant voltage
    rcl repeller         ;set the repeller to the desired pulsed value
    sto Adj_elect01
    rcl flight_tube      ;set the flight_tube to the desired
    sto Adj_elect03      ;pulsed value
    exit

    lbl start_voltages   ;starting voltages
    0
    sto Adj_elect01      ;set repeller and flight tube
    sto Adj_elect03      ;voltages to zero
    exit

;-----transition color control-----

seg Other_actions
    rcl Next_PE_Update   ;recall time for next PE update
    rcl Ion_time_of_flight ;recall ion's time of flight
    x<y goto next_test   ;if the tof is les than next pe update
    rcl PE_update        ;recall pe update increment
    + sto next_pe_update ;add to tof and store as next pe update
    1 sto update_pe_surface ;request a pe surface update

    lbl next_test
    rcl Ion_time_of_flight ;get ion's time of flight
    rcl tmark             ;recall transition time
    x!=y exit            ;exit if not at transition
    rcl color sto Ion_color ;set ion's after transition color

```



### A.3. Br<sup>+</sup> Curve Fits at T<sub>s</sub> = 25° C

The following graphs represent the results from a series of curve fits to Br<sup>+</sup> product velocity-, polar- intensity, and polar energy- distributions described in Sect. 3.3.2 for Br<sup>+</sup> scattered on Pt(111) at 25° C across the 14 eV – 104 eV incident energy range. Briefly, the velocity distributions shown in Figures A.3.1-A.3.13 (a) are fit to a series of three Gaussian functions,  $\square$ ,  $\square$ , and  $\square$  according to equation 3.2. For the polar intensity plots in Figures A.3.1-A.3.13 (b), the  $\square$ ,  $\square$ , and  $\square$  components are calculated according to equation 3.6 with the width parameter,  $n_i$ , for each component held constant across the incident energy range. The polar energy curve fits are calculated from the polar intensity fits and the average energy values obtained from the velocity distribution fits.

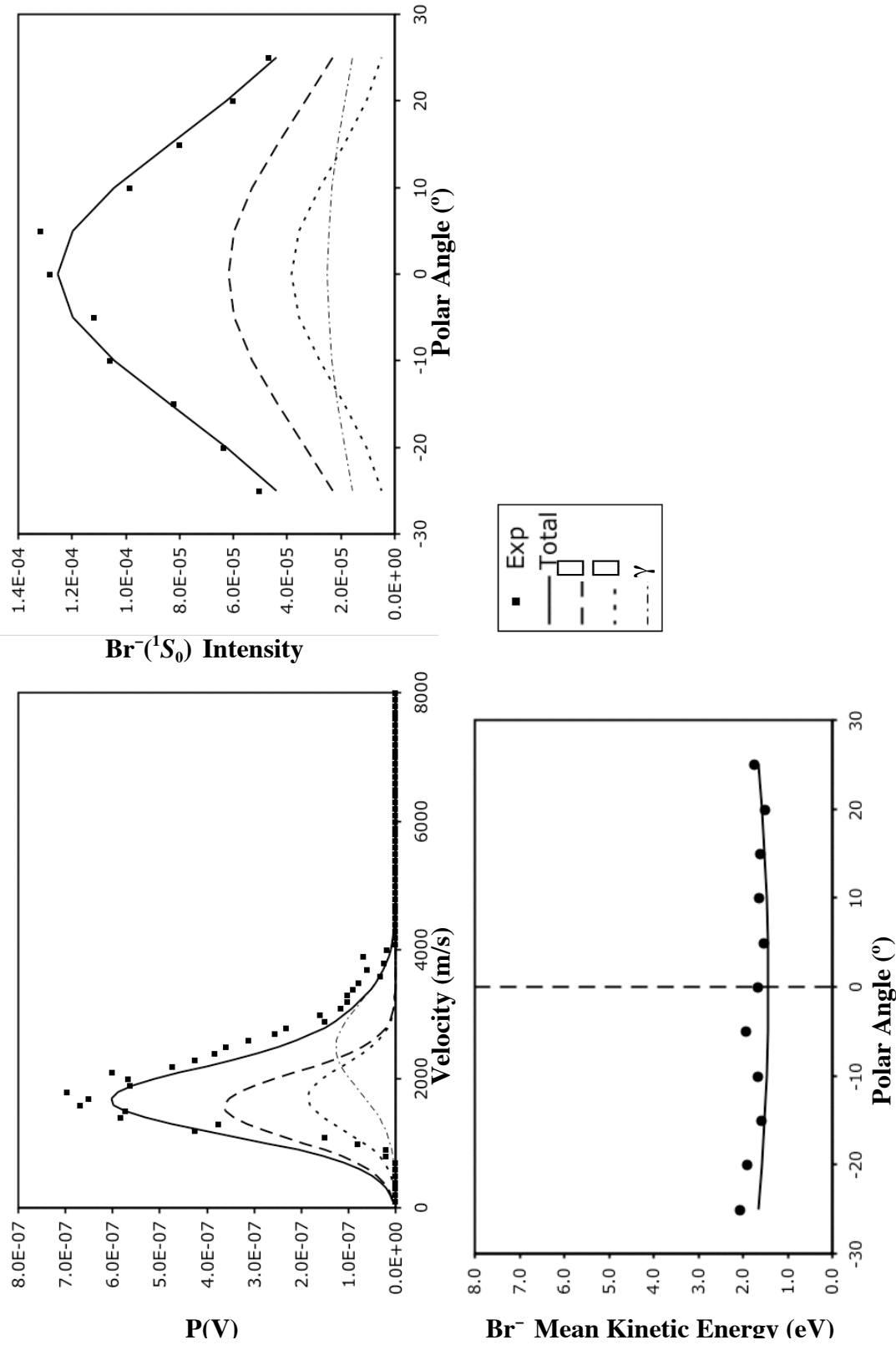


Figure A.3.1.  $\text{Br}^-(^1S_0)$  (a) product velocity distributions (b) polar intensity distribution and (c) polar energy distribution for 14 eV incident  $\text{Br}^+(^3P_2)$  collision energy on Pt(111) at  $T_s = 25^\circ\text{C}$ . The  $\square$ ,  $\Delta$ , and  $\gamma$  components are calculated according to equations 3.2 and 3.6. The solid lines that represent the sum of the three components is compared to the data in each plot.

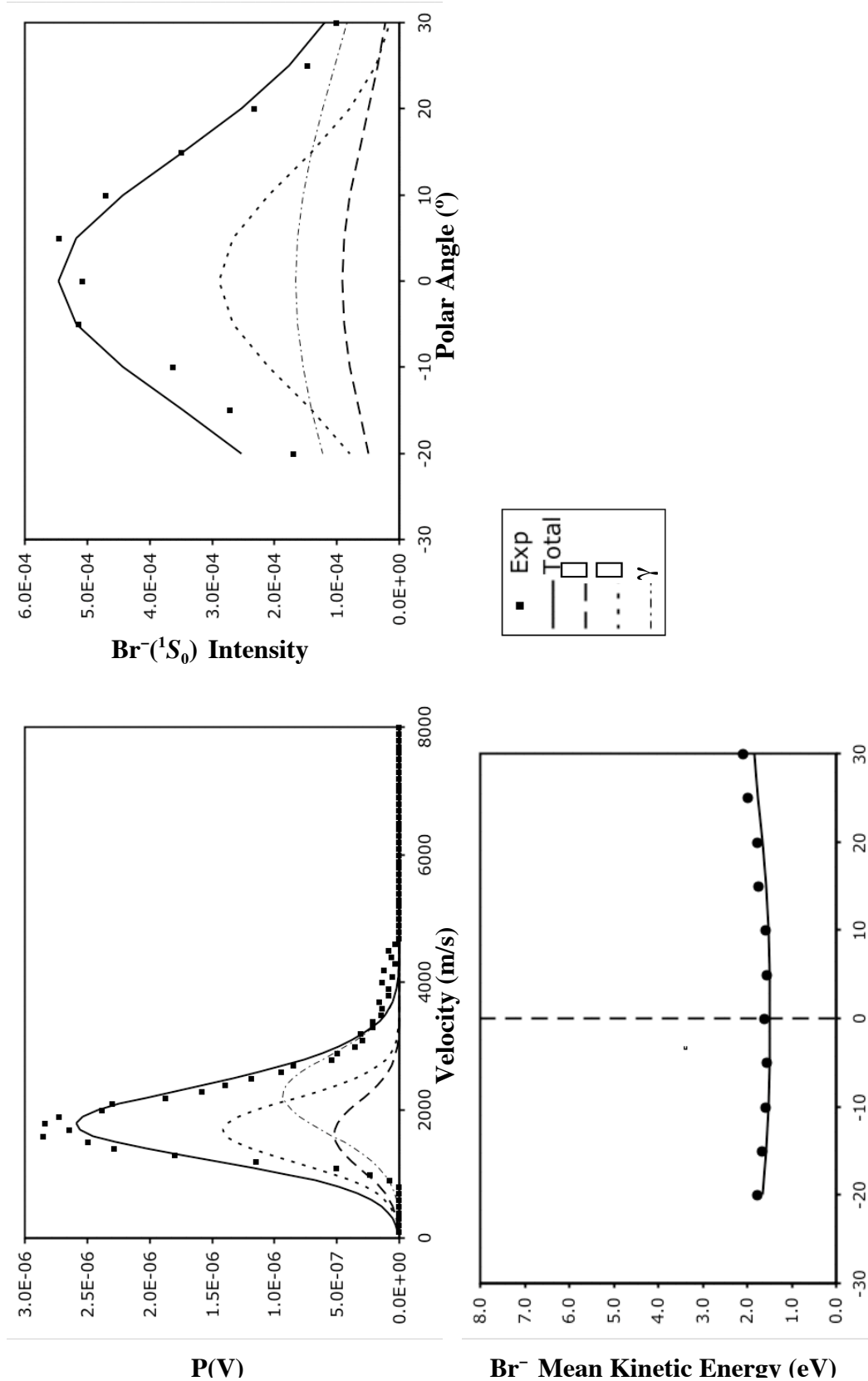


Figure A.3.2.  $Br^{-}(^1S_0)$  (a) product velocity distributions (b) polar intensity distribution and (c) polar energy distribution for 19 eV incident  $Br^{+}(^3P_2)$  collision energy on Pt(111) at  $T_s = 25^{\circ}C$ . The  $\square$ ,  $\square$ , and  $\gamma$  components are calculated according to equations 3.2 and 3.6. The solid lines that represent the sum of the three components is compared to the data in each plot.

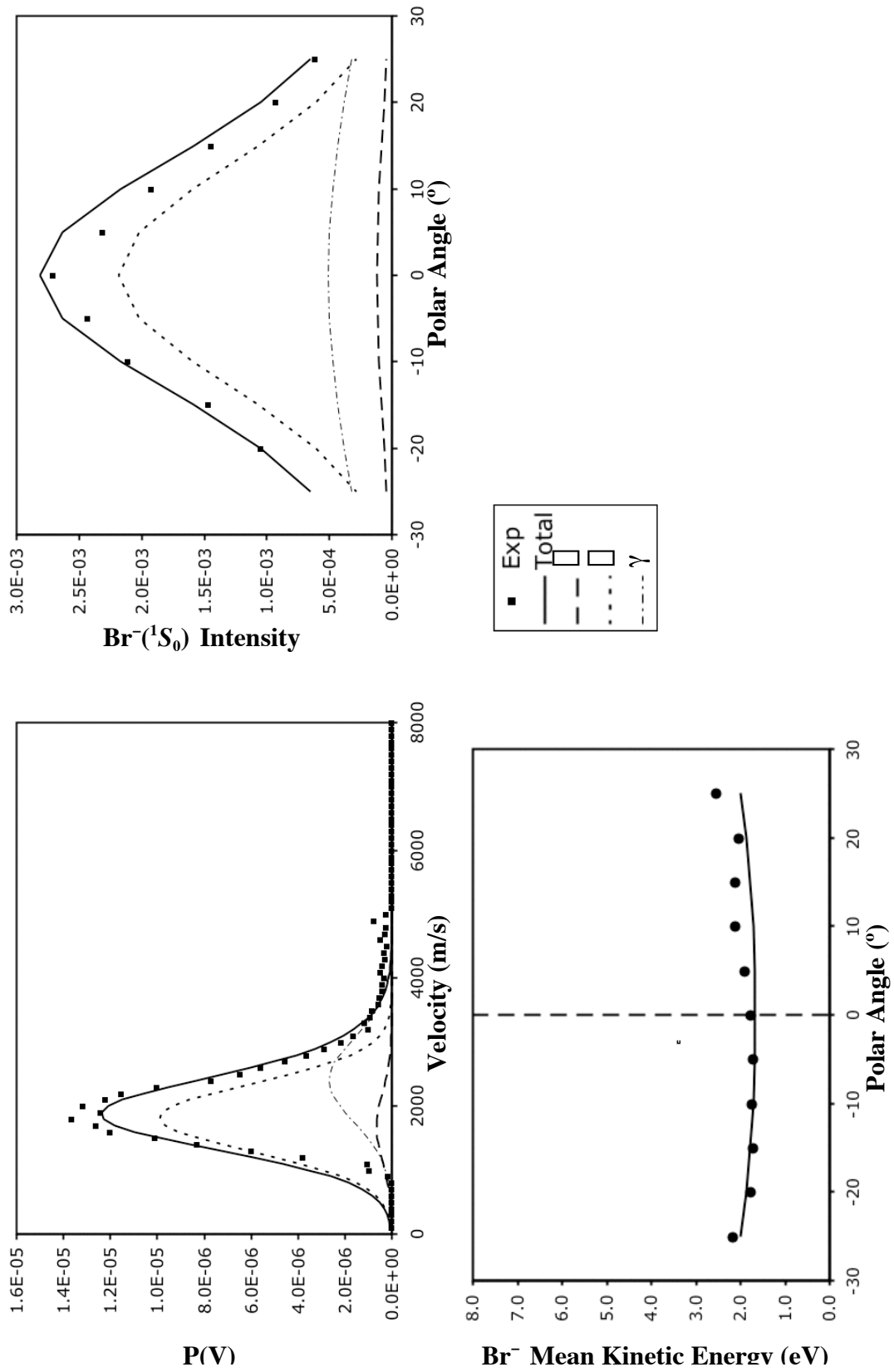


Figure A.3.3. Br<sup>-</sup>(<sup>1</sup>S<sub>0</sub>) (a) product velocity distributions (b) polar intensity distribution and (c) polar energy distribution for 21.5 eV incident Br<sup>+</sup>(<sup>3</sup>P<sub>2</sub>) collision energy on Pt(111) at T<sub>s</sub> = 25° C. The □, ▢, and γ components are calculated according to equations 3.2 and 3.6. The solid lines that represent the sum of the three components is compared to the data in each plot.

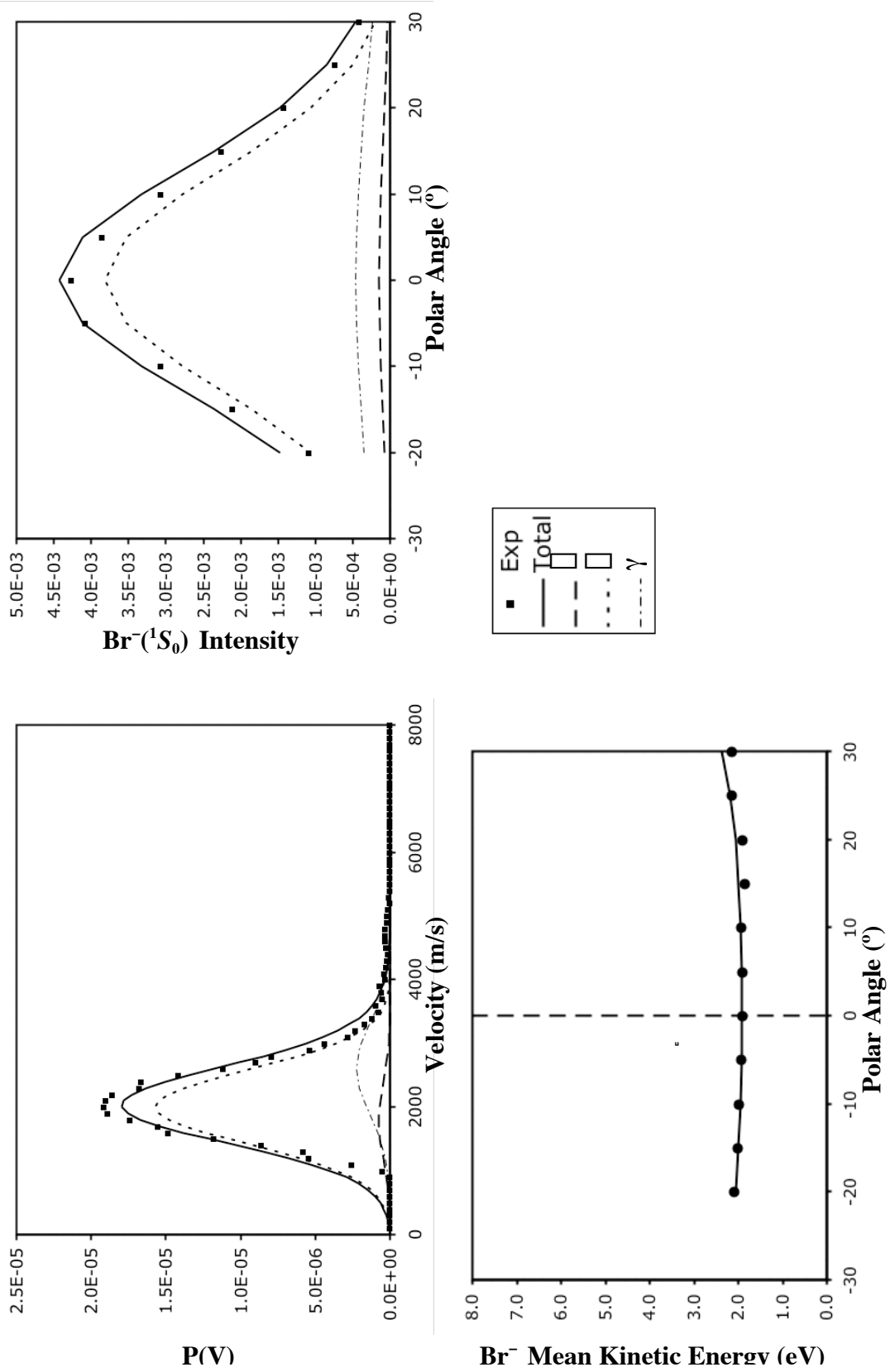


Figure A.3.4.  $\text{Br}^-({}^1S_0)$  (a) product velocity distributions (b) polar intensity distribution and (c) polar energy distribution for 24 eV incident  $\text{Br}^+({}^3P_2)$  collision energy on Pt(111) at  $T_s = 25^\circ\text{C}$ . The  $\square$ ,  $\square$ , and  $\gamma$  components are calculated according to equations 3.2 and 3.6. The solid lines that represent the sum of the three components is compared to the data in each plot.

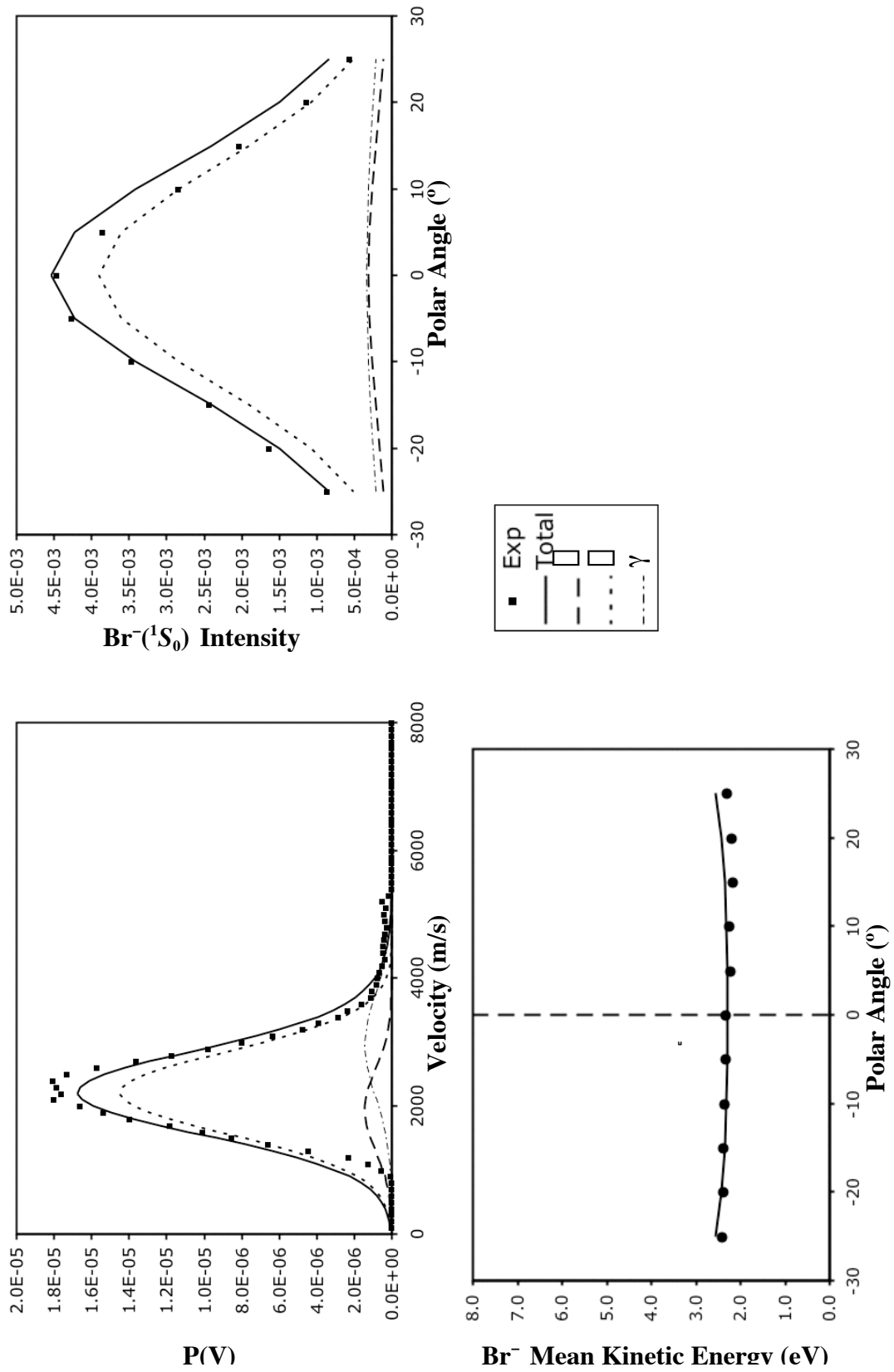


Figure A.3.5.  $\text{Br}^-(^1S_0)$  (a) product velocity distributions (b) polar intensity distribution and (c) polar energy distribution for 29 eV incident  $\text{Br}^+(^3P_2)$  collision energy on Pt(111) at  $T_s = 25^\circ\text{C}$ . The  $\square$ ,  $\square$ , and  $\square$  components are calculated according to equations 3.2 and 3.6. The solid lines that represent the sum of the three components is compared to the data in each plot.

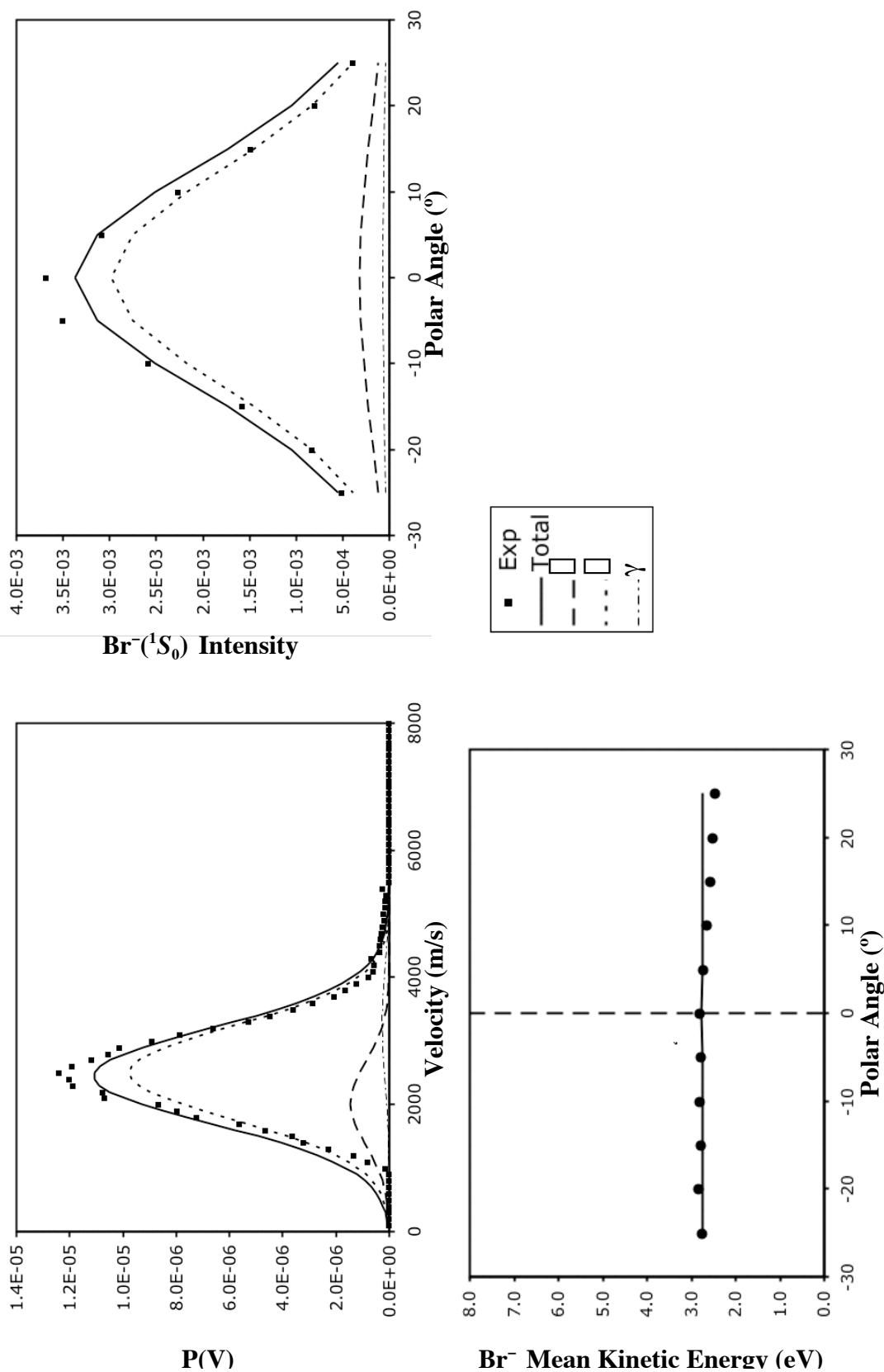


Figure A.3.6.  $\text{Br}^-({}^1S_0)$  (a) product velocity distributions (b) polar intensity distribution and (c) polar energy distribution for 34 eV incident  $\text{Br}^+({}^3P_2)$  collision energy on Pt(111) at  $T_s = 25^\circ\text{C}$ . The  $\square$ ,  $\square$ , and  $\square$  components are calculated according to equations 3.2 and 3.6. The solid lines that represent the sum of the three components is compared to the data in each plot.

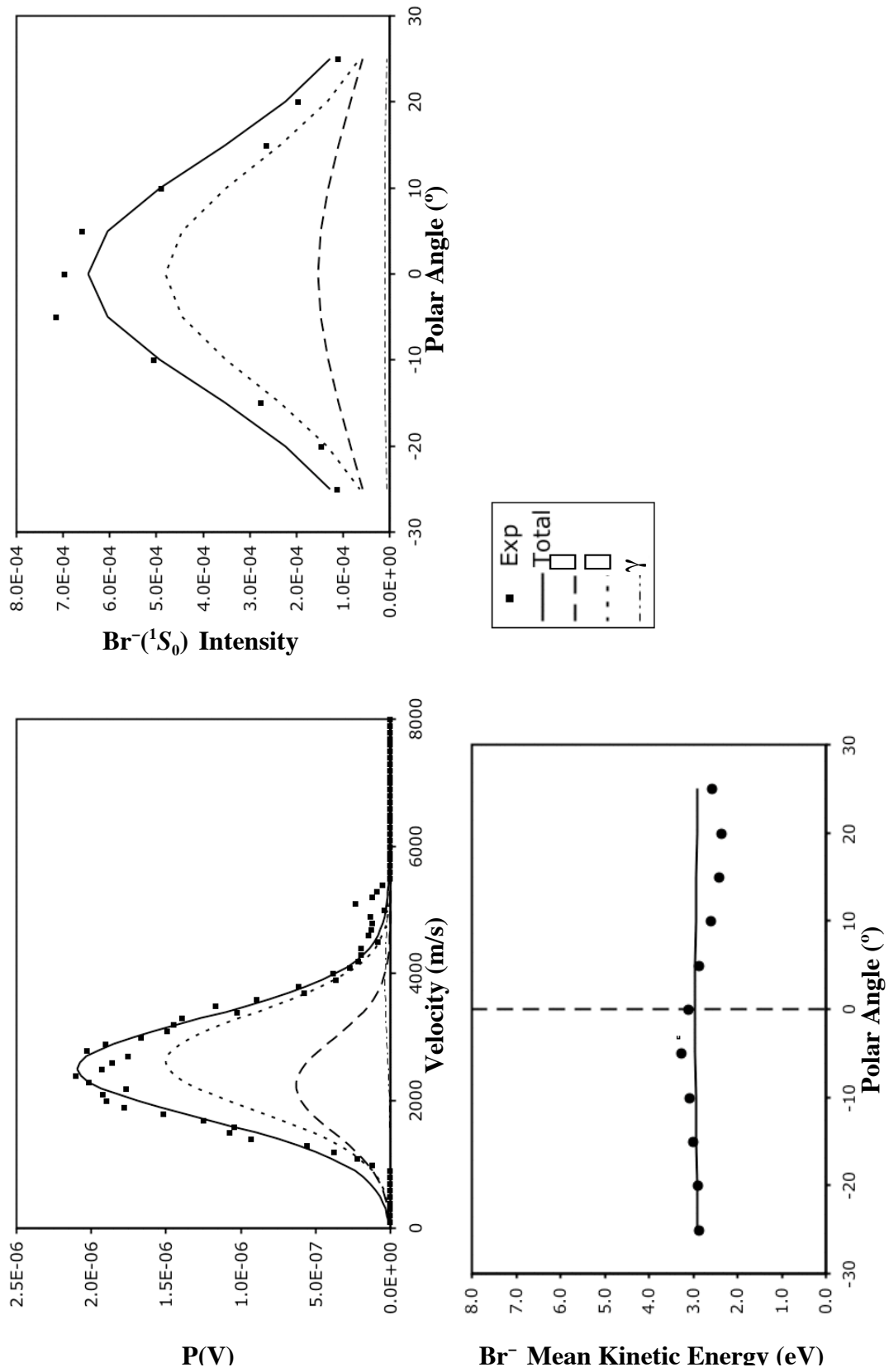


Figure A.3.7.  $\text{Br}^-(^1S_0)$  (a) product velocity distributions (b) polar intensity distribution and (c) polar energy distribution for 44 eV incident  $\text{Br}^+(^3P_2)$  collision energy on  $\text{Pt}(111)$  at  $T_s = 25^\circ\text{C}$ . The  $\square$ ,  $\square$ , and  $\square$  components are calculated according to equations 3.2 and 3.6. The solid lines that represent the sum of the three components is compared to the data in each plot.



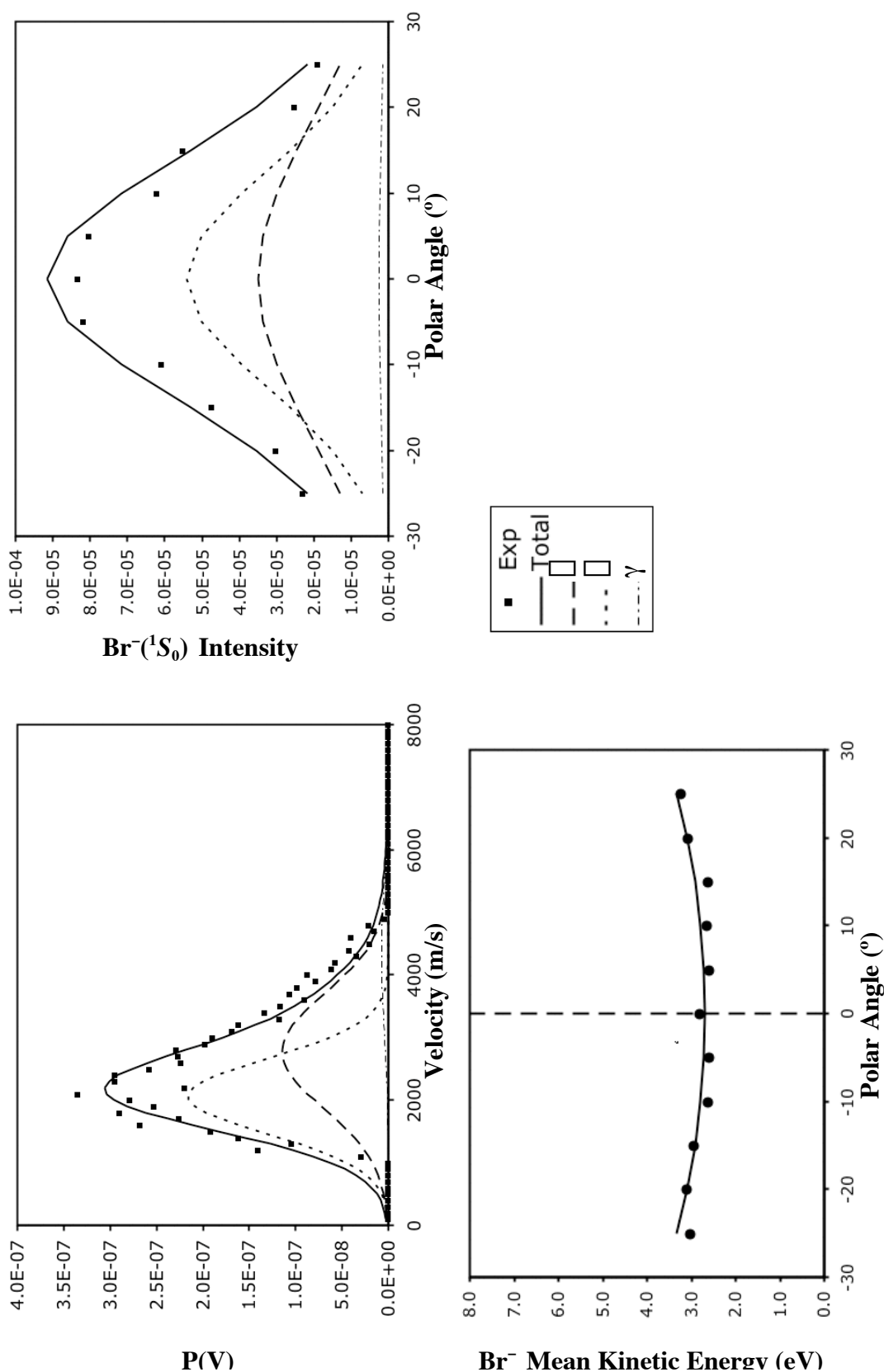


Figure A.3.8.  $\text{Br}^-(^1S_0)$  (a) product velocity distributions (b) polar intensity distribution and (c) polar energy distribution for 54 eV incident  $\text{Br}^+(^3P_2)$  collision energy on Pt(111) at  $T_s = 25^\circ\text{C}$ . The  $\square$ ,  $\square$ , and  $\square$  components are calculated according to equations 3.2 and 3.6. The solid lines that represent the sum of the three components is compared to the data in each plot.

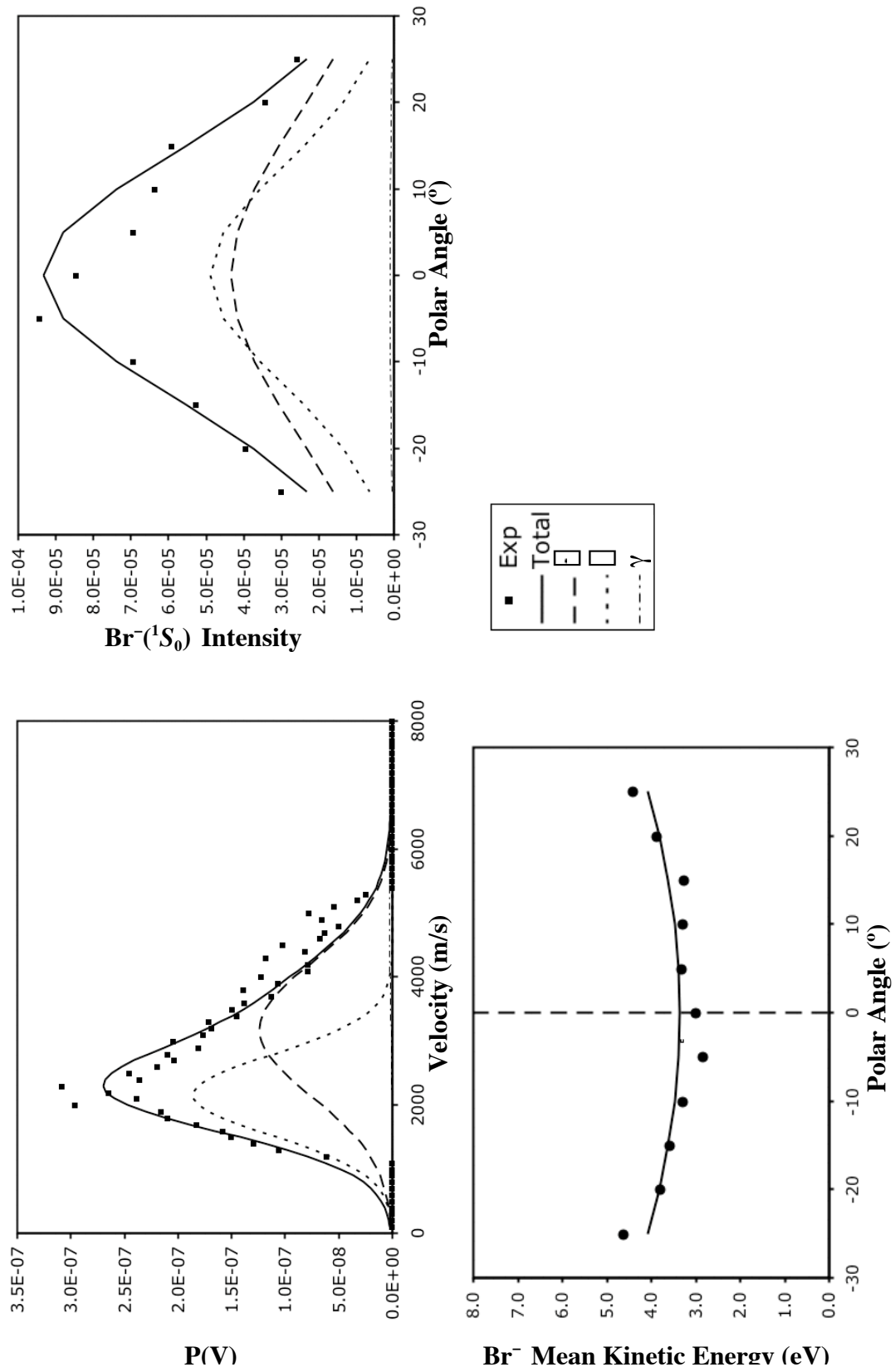


Figure A.3.9.  $Br^{-}(^1S_0)$  (a) product velocity distributions (b) polar intensity distribution and (c) polar energy distribution for 64 eV incident  $Br^{+}(^3P_2)$  collision energy on Pt(111) at  $T_s = 25^{\circ}C$ . The  $\square$ ,  $\square$ , and  $\gamma$  components are calculated according to equations 3.2 and 3.6. The solid lines that represent the sum of the three components is compared to the data in each plot.

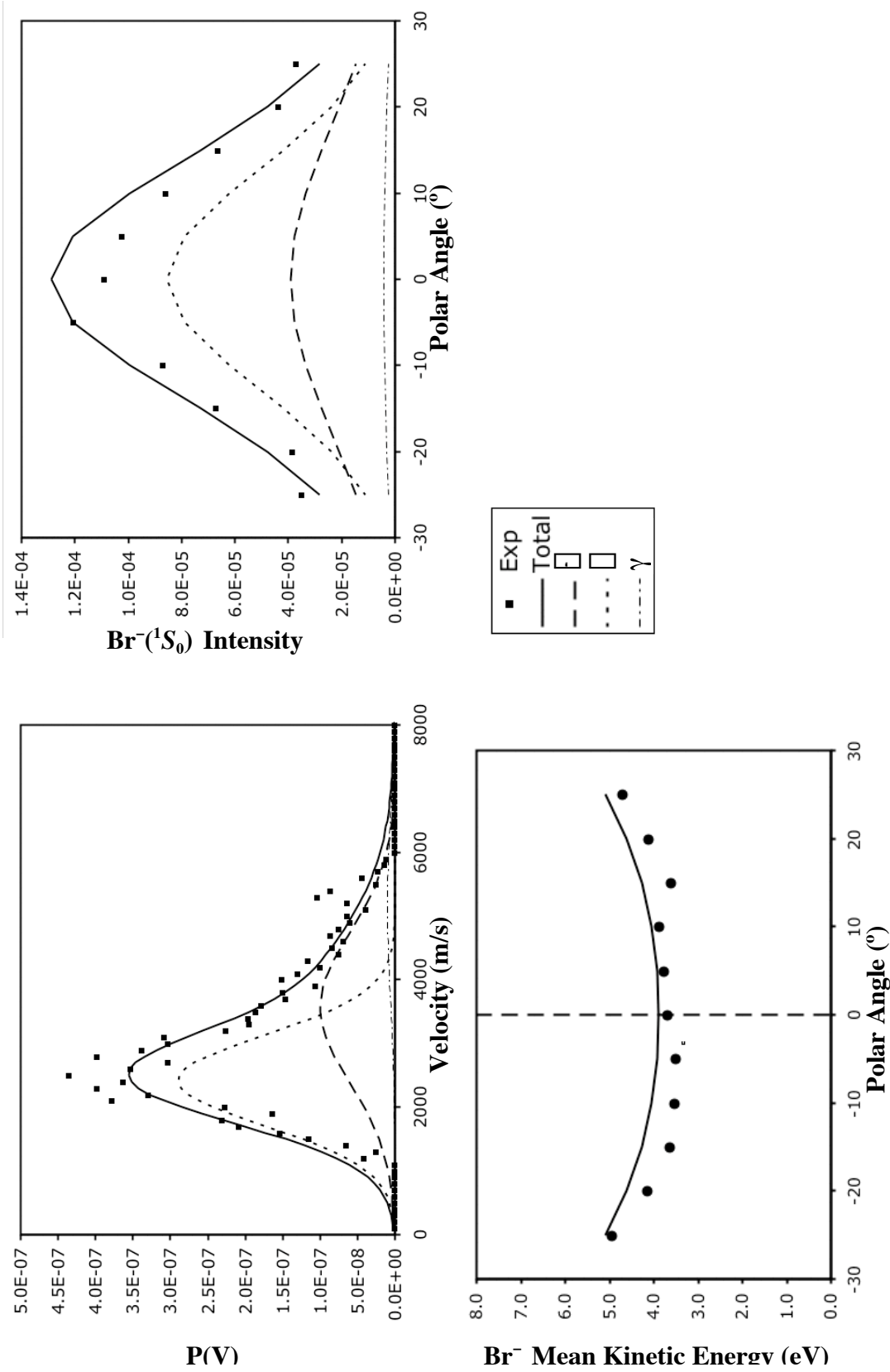


Figure A.3.10. Br<sup>-</sup>(<sup>1</sup>S<sub>0</sub>) (a) product velocity distributions (b) polar intensity distribution and (c) polar energy distribution for 74 eV incident Br<sup>+</sup>(<sup>3</sup>P<sub>2</sub>) collision energy on Pt(111) at T<sub>s</sub> = 25° C. The  $\square$ ,  $\square$ ,  $\square$ , and  $\square$  components are calculated according to equations 3.2 and 3.6. The solid lines that represent the sum of the three components is compared to the data in each plot.

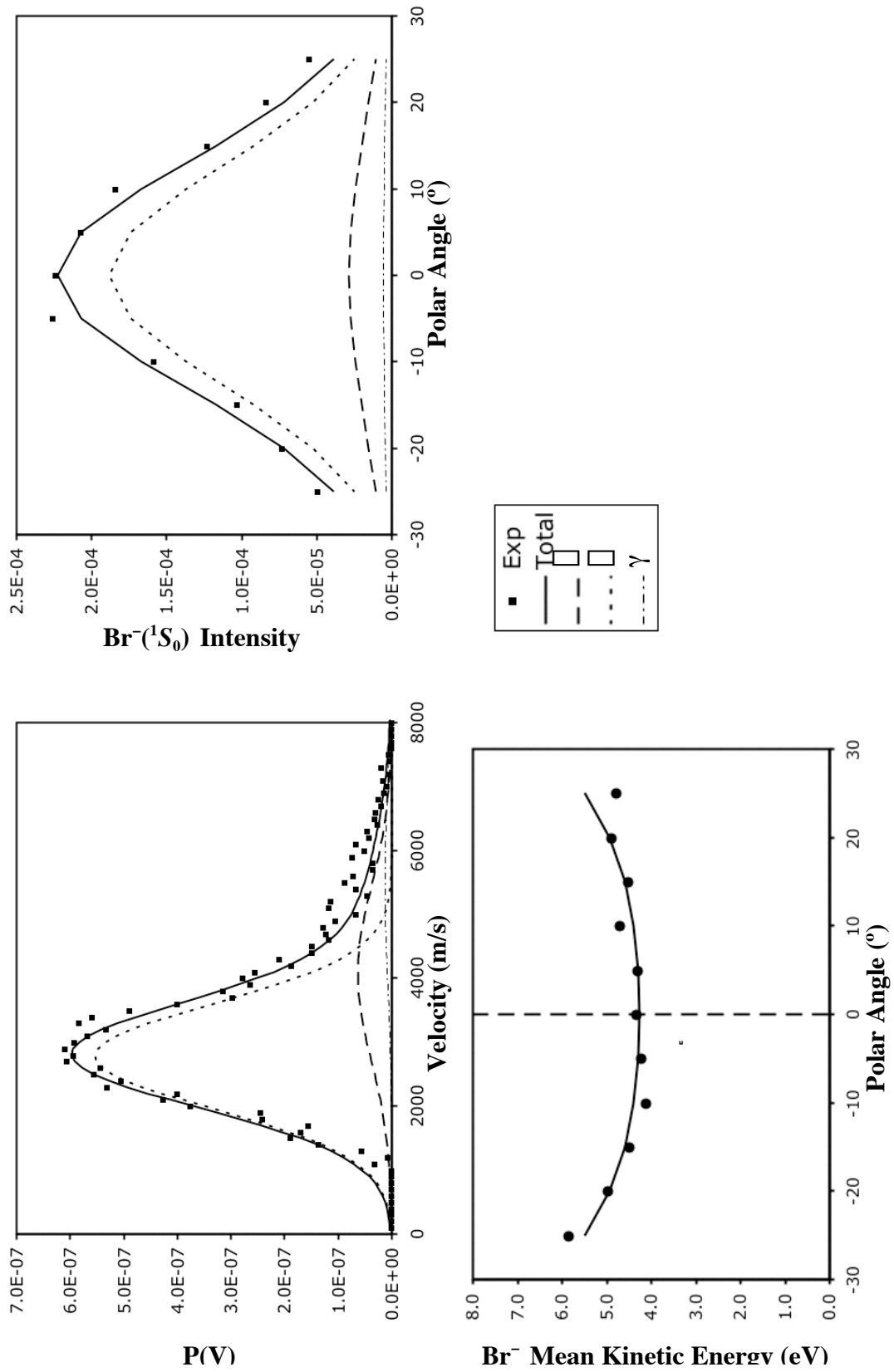


Figure A.3.11.  $\text{Br}^-(^1S_0)$  (a) product velocity distributions (b) polar intensity distribution and (c) polar energy distribution for 84 eV incident  $\text{Br}^+(^3P_2)$  collision energy on Pt(111) at  $T_s = 25^\circ \text{C}$ . The  $\square$ ,  $\square$ , and  $\gamma$  components are calculated according to equations 3.2 and 3.6. The solid lines that represent the sum of the three components is compared to the data in each plot.

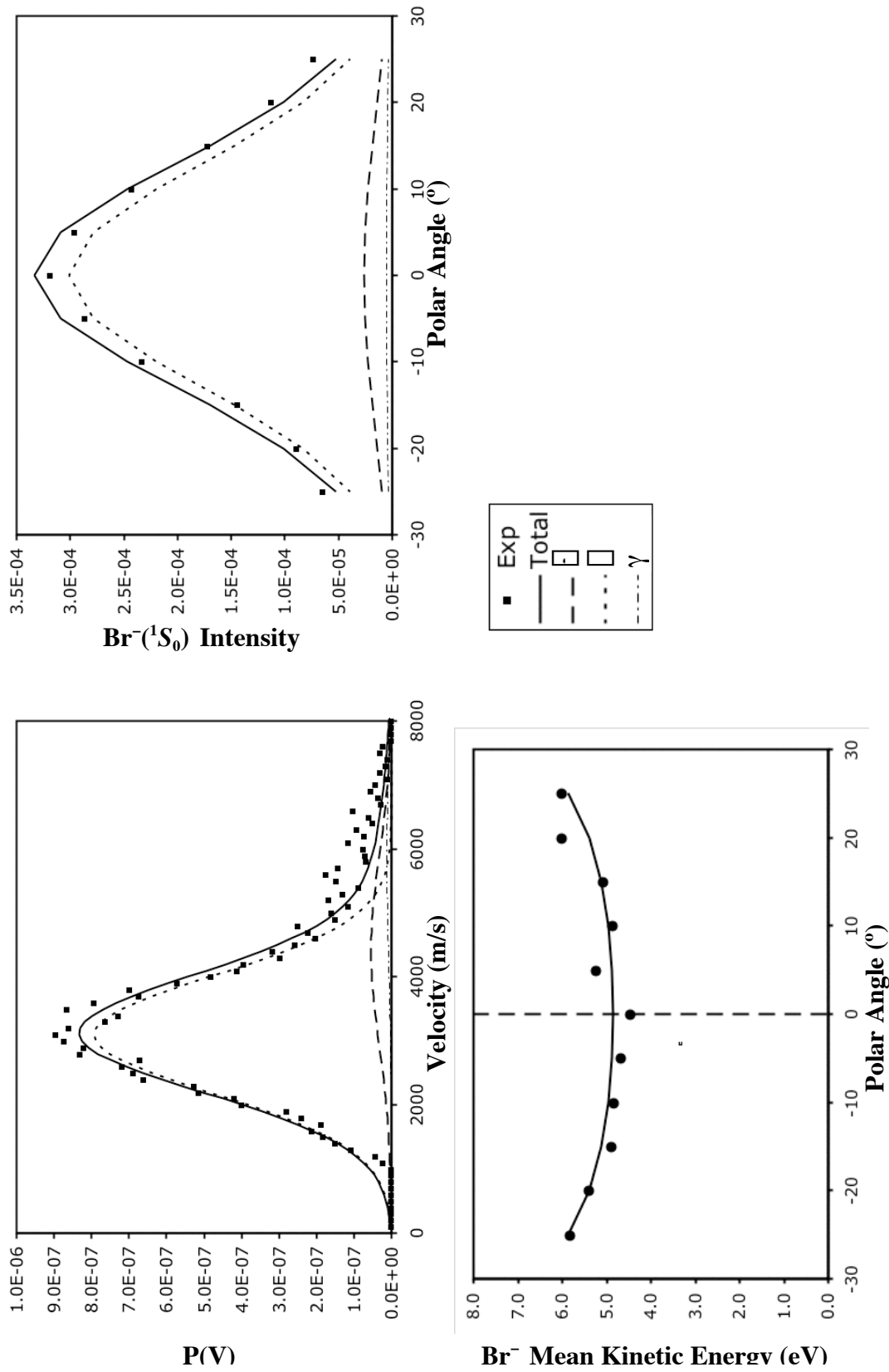


Figure A.3.12.  $\text{Br}^-(^1S_0)$  (a) product velocity distributions (b) polar intensity distribution and (c) polar energy distribution for 94 eV incident  $\text{Br}^+(^3P_2)$  collision energy on Pt(111) at  $T_s = 25^\circ\text{C}$ . The  $\square$ ,  $\square$ , and  $\square$  components are calculated according to equations 3.2 and 3.6. The solid lines that represent the sum of the three components is compared to the data in each plot.

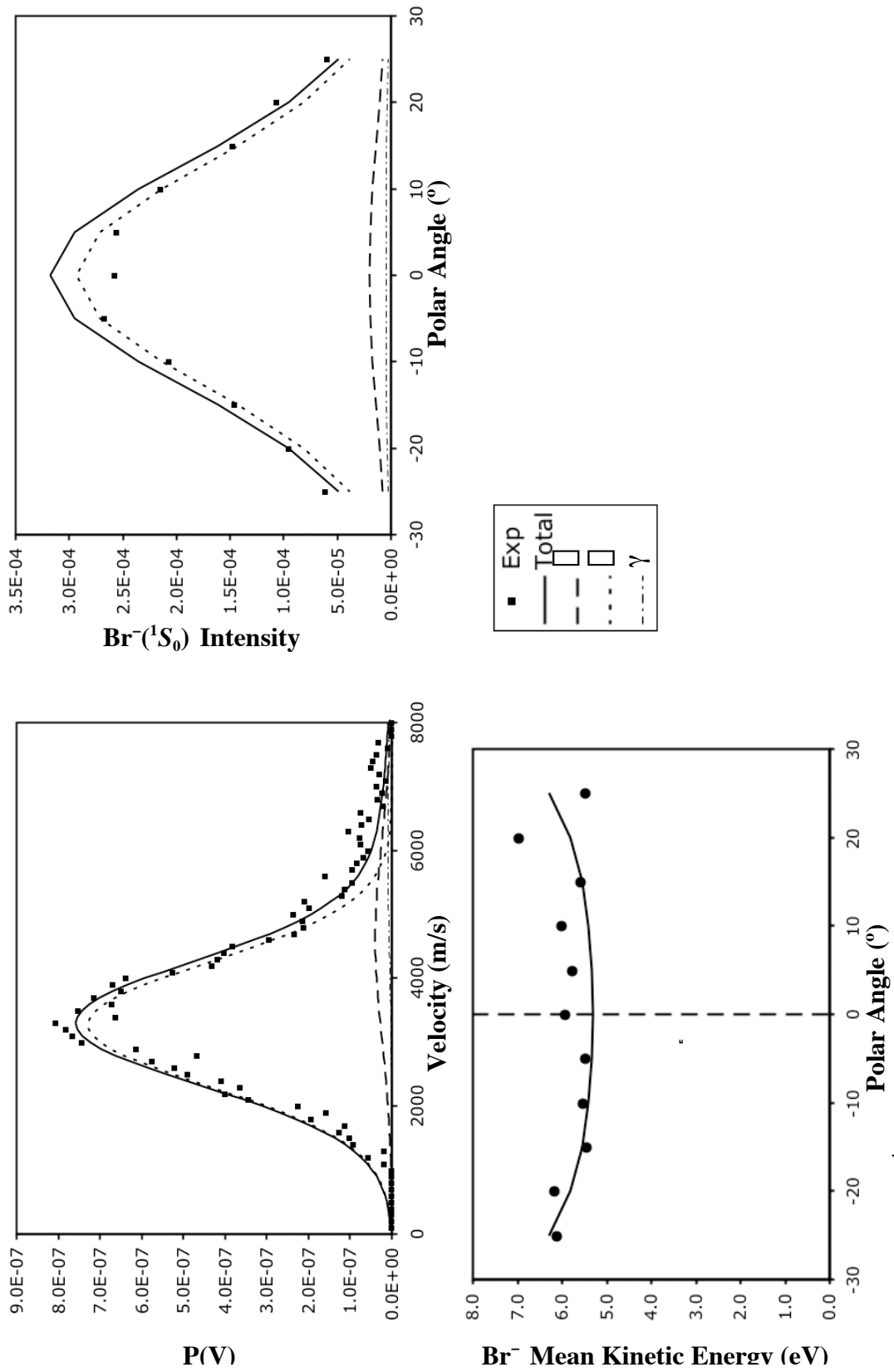


Figure A.3.13.  $\text{Br}^-(^1S_0)$  (a) product velocity distributions (b) polar intensity distribution and (c) polar energy distribution for 104 eV incident  $\text{Br}^+(^3P_2)$  collision energy on Pt(111) at  $T_s = 25^\circ \text{C}$ . The  $\square$ ,  $\square$ , and  $\gamma$  components are calculated according to equations 3.2 and 3.6. The solid lines that represent the sum of the three components is compared to the data in each plot.

#### A.4. Br<sup>+</sup> Polar Velocity Maps at T<sub>s</sub> = 25° C

The following graphs compare the parameterized fits to the experimental data for Br<sup>-</sup>(<sup>1</sup>S<sub>0</sub>) products when Br<sup>+</sup> scatters on Pt(111) at 25° C. Figures 3.14-3.17 only represent the data and calculated polar velocity maps for 29, 44, 64, and 84 eV collision energies, respectively. This appendix completes the data set for the 14 – 104 eV Br<sup>+</sup> incident energy range. Briefly, the fitting parameters obtained from the Br<sup>-</sup>(<sup>1</sup>S<sub>0</sub>) velocity- and polar-distributions are combined to calculate the polar velocity maps for each of the components,  $\hat{v}_x$ ,  $\hat{v}_y$ , and  $\hat{v}_z$  according to equation 3.9 and the results are shown in A.4.1-A.4.10 (c), (d), and (e), respectively. For each collision energy, the sum of the polar velocity maps for the three components is calculated according to equations 3.10 and the results are shown in A.4.1-A.4.10 (b),

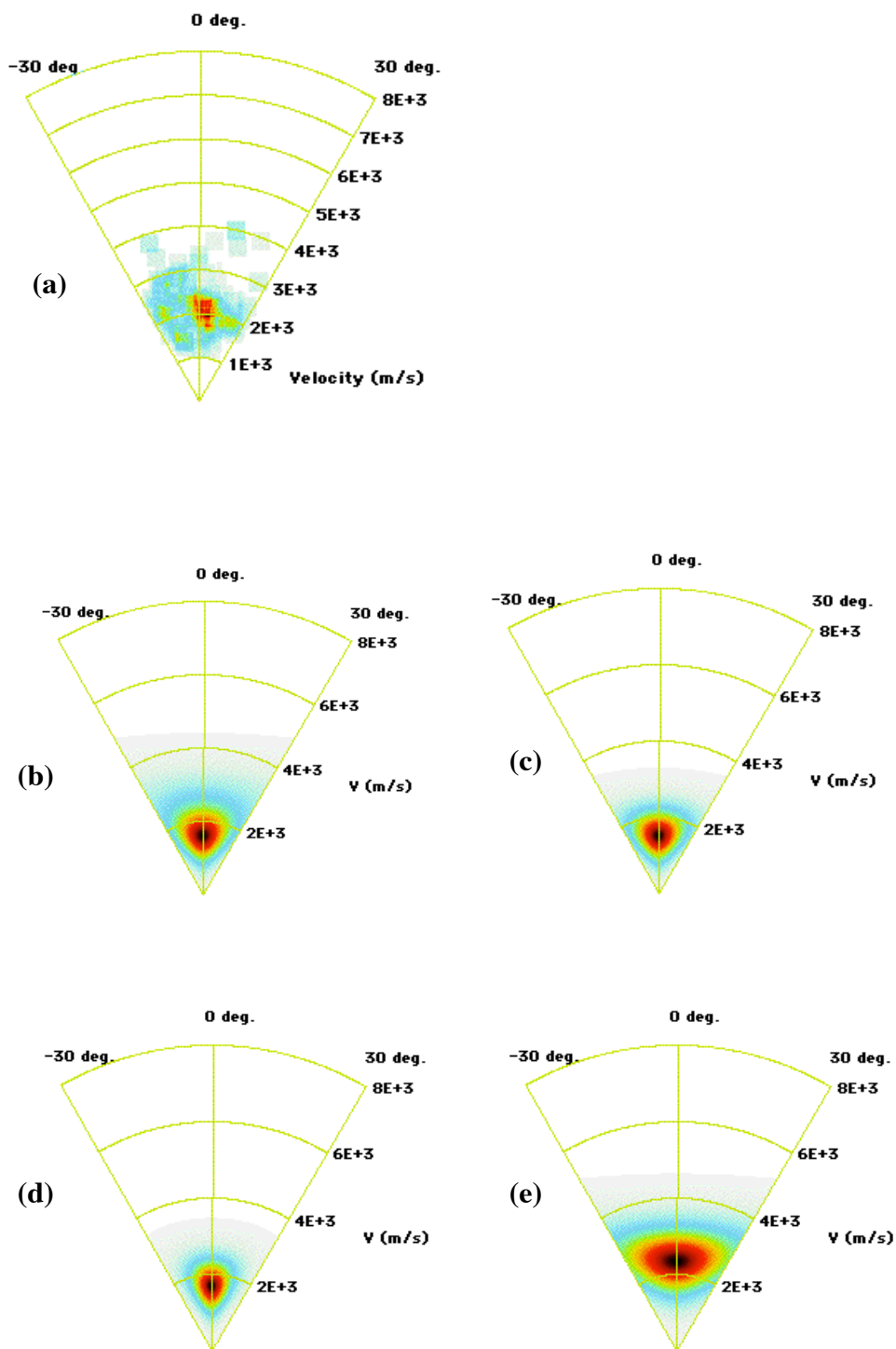


Figure A.4.1. Comparison of the parameterized fits to the experimental data for the  $\text{Br}^-(^1S_0)$  product intensity versus polar exit velocity at 11 eV incident energy. (a) Experimental data and (b) parameterized fit all three components combined, (c)  $\bar{\gamma}$  component only, (d)  $\bar{\gamma}$  component only, and (e)  $\bar{\gamma}$  component only. Red indicates the highest product yield and white indicates the lowest intensity.



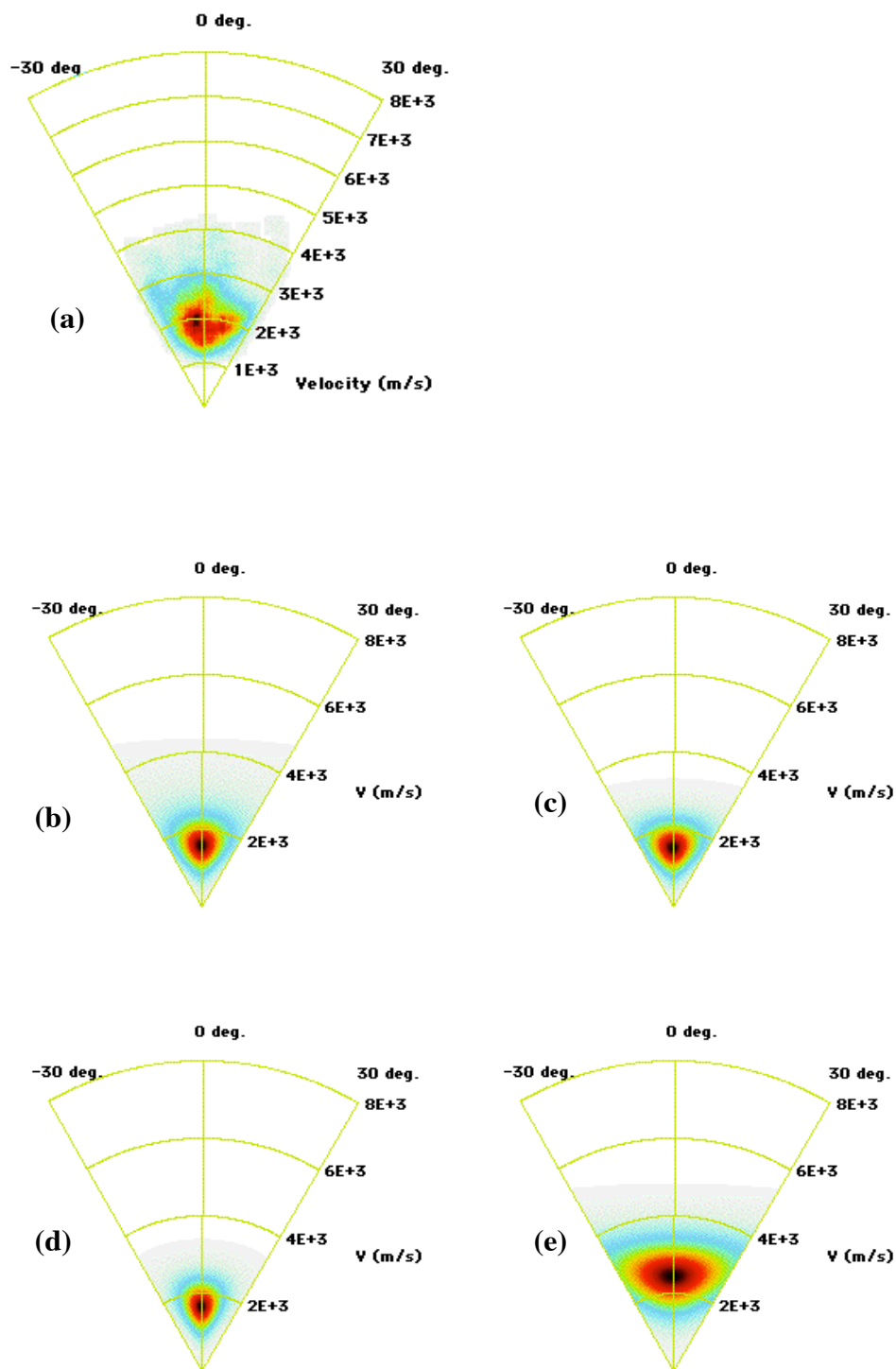


Figure A.4.2. Comparison of the parameterized fits to the experimental data for the  $\text{Br}^-(^1S_0)$  product intensity versus polar exit velocity at 14 eV incident energy. (a) Experimental data and (b) parameterized fit all three components combined, (c)  $\bar{\gamma}$  component only, (d)  $\bar{\gamma}$  component only, and (e)  $\bar{\gamma}$  component only. Red indicates the highest product yield and white indicates the lowest intensity.

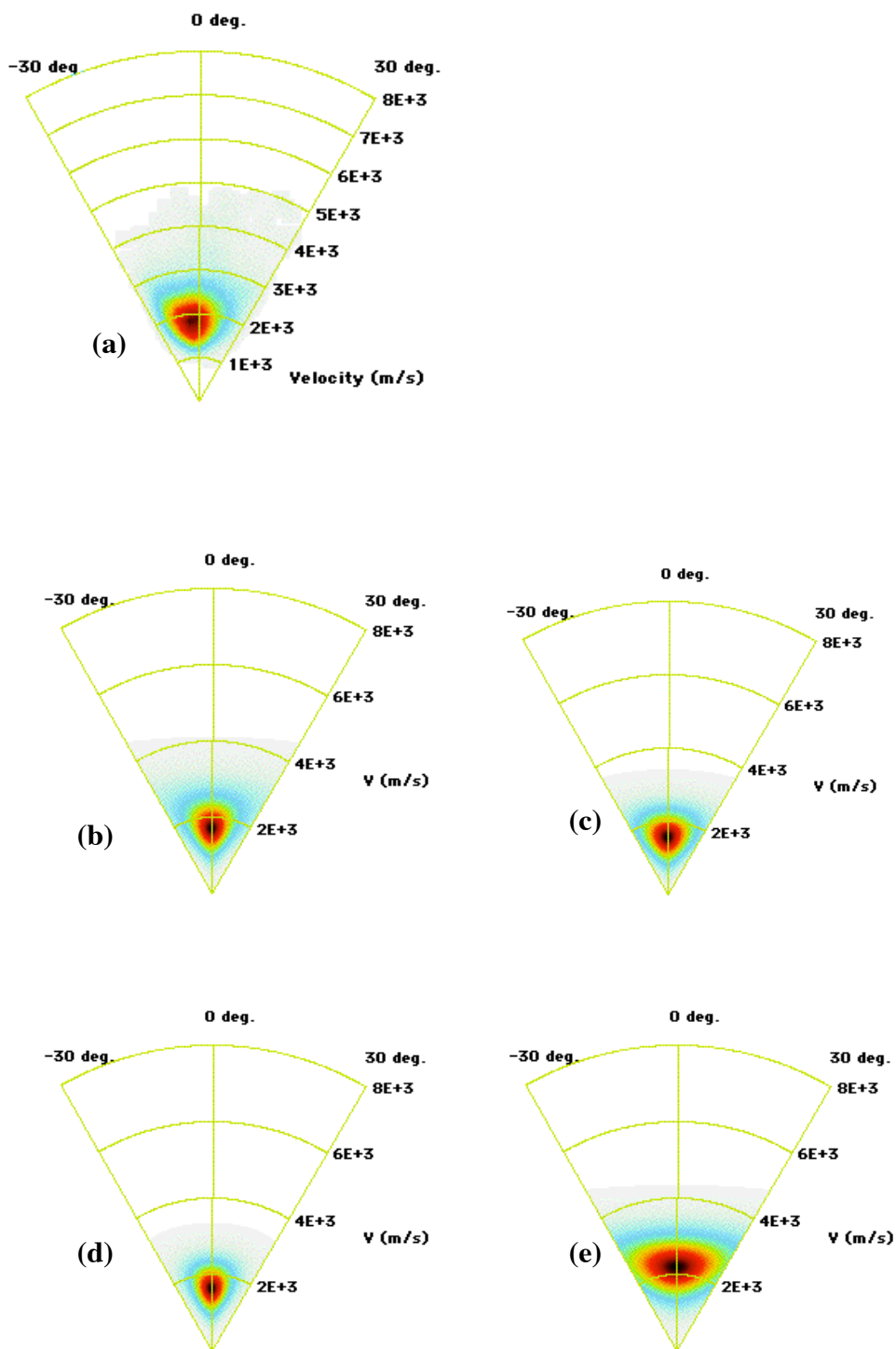


Figure A.4.3. Comparison of the parameterized fits to the experimental data for the  $\text{Br}^-(^1S_0)$  product intensity versus polar exit velocity at 19 eV incident energy. (a) Experimental data and (b) parameterized fit all three components combined, (c)  $\bar{\gamma}$  component only, (d)  $\bar{\gamma}$  component only, and (e)  $\bar{\gamma}$  component only. Red indicates the highest product yield and white indicates the lowest intensity.

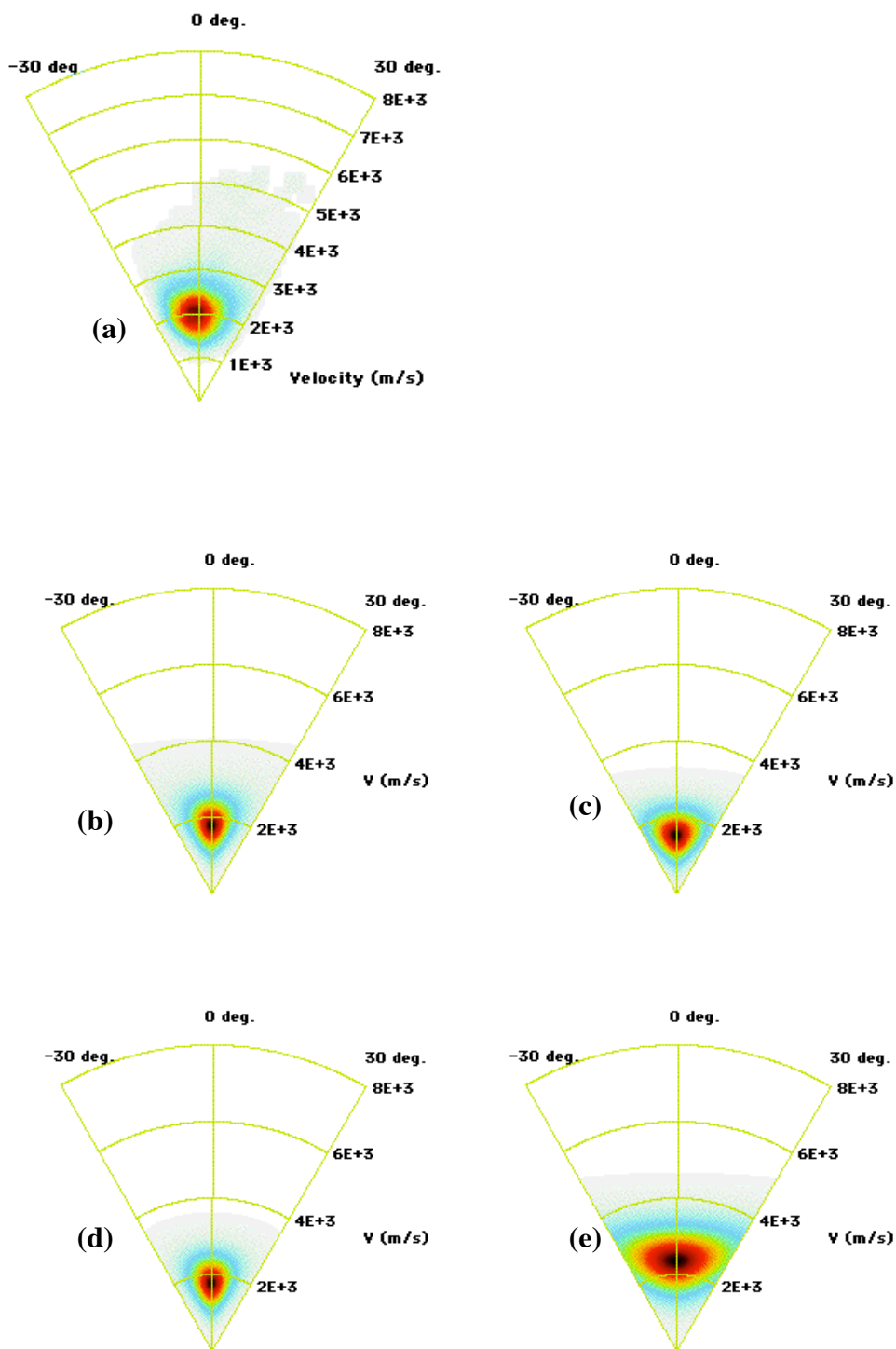


Figure A.4.4. Comparison of the parameterized fits to the experimental data for the  $\text{Br}^-(^1S_0)$  product intensity versus polar exit velocity at 21.5 eV incident energy. (a) Experimental data and (b) parameterized fit all three components combined, (c)  $\bar{\gamma}$  component only, (d)  $\bar{\gamma}$  component only, and (e)  $\bar{\gamma}$  component only. Red indicates the highest product yield and white indicates the lowest intensity.

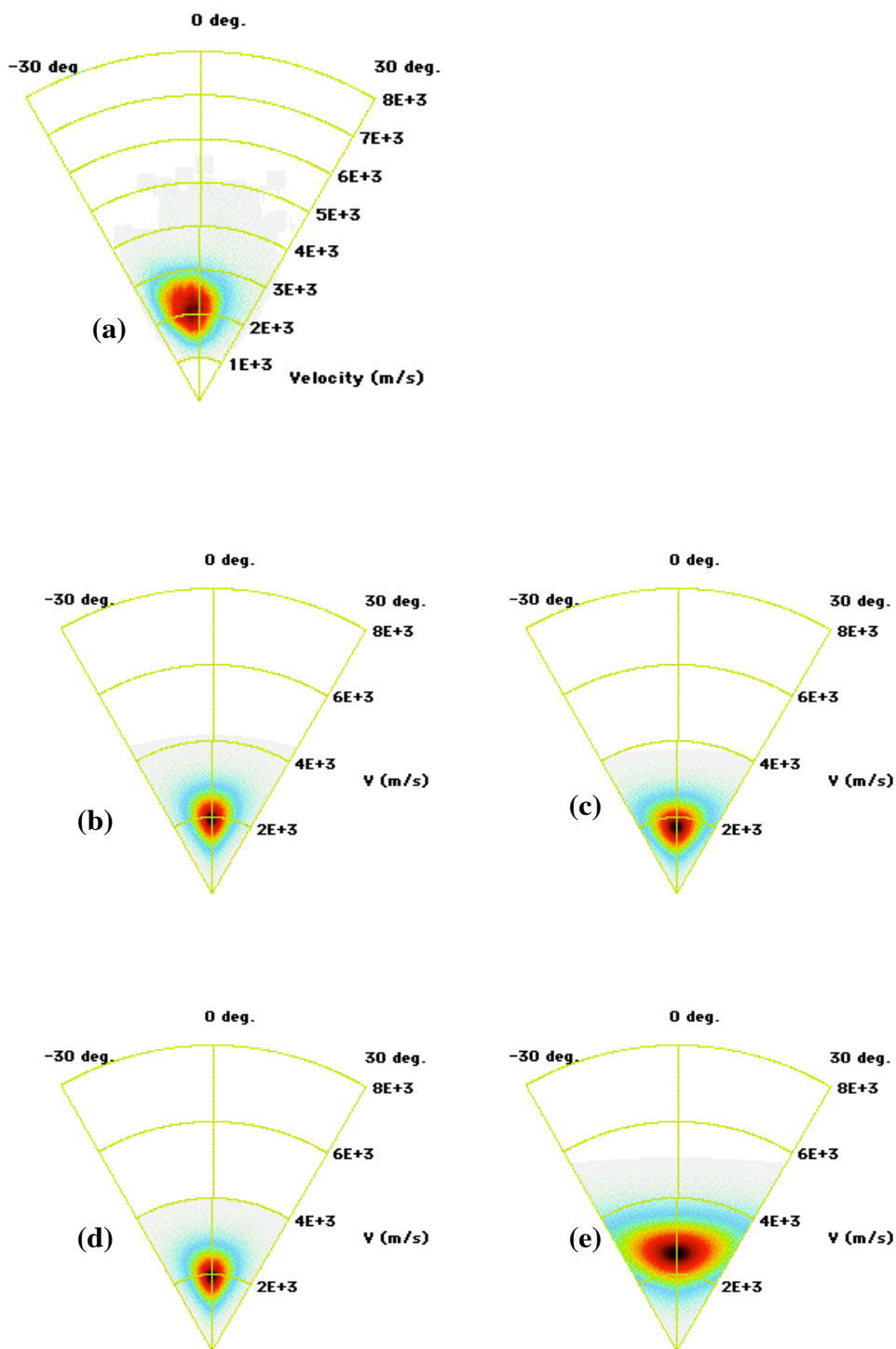


Figure A.4.5. Comparison of the parameterized fits to the experimental data for the  $\text{Br}^-(^1S_0)$  product intensity versus polar exit velocity at 24 eV incident energy. (a) Experimental data and (b) parameterized fit all three components combined, (c)  $\bar{\gamma}$  component only, (d)  $\bar{\gamma}$  component only, and (e)  $\bar{\gamma}$  component only. Red indicates the highest product yield and white indicates the lowest intensity.

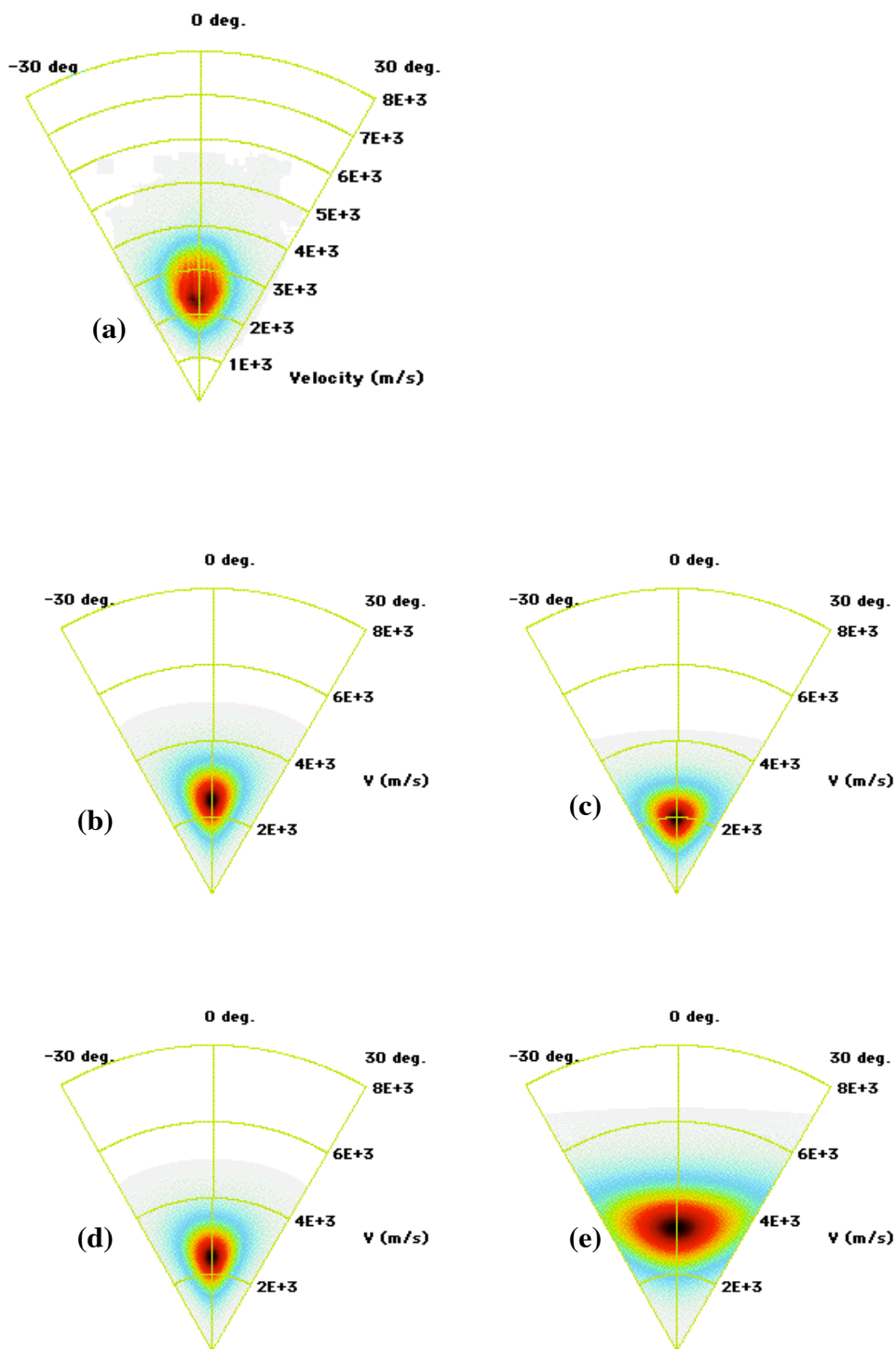


Figure A.4.6. Comparison of the parameterized fits to the experimental data for the  $\text{Br}^-(^1S_0)$  product intensity versus polar exit velocity at 34 eV incident energy. (a) Experimental data and (b) parameterized fit all three components combined, (c)  $\bar{\sigma}$  component only, (d)  $\bar{\sigma}$  component only, and (e)  $\bar{\sigma}$  component only. Red indicates the highest product yield and white indicates the lowest intensity.

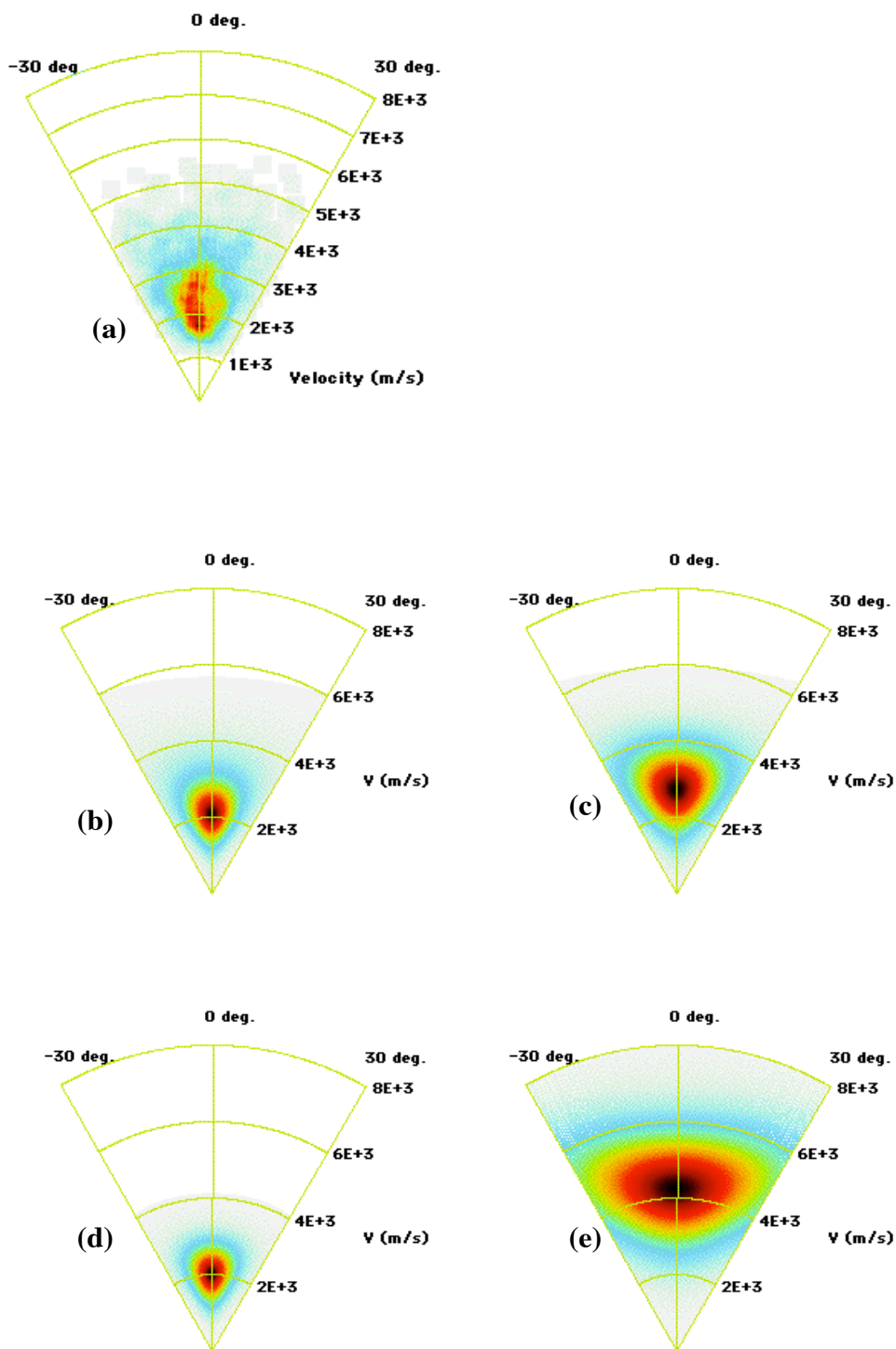


Figure A.4.7. Comparison of the parameterized fits to the experimental data for the  $\text{Br}^-(^1S_0)$  product intensity versus polar exit velocity at 54 eV incident energy. (a) Experimental data and (b) parameterized fit all three components combined, (c)  $\bar{\gamma}$  component only, (d)  $\bar{\gamma}$  component only, and (e)  $\bar{\gamma}$  component only. Red indicates the highest product yield and white indicates the lowest intensity.

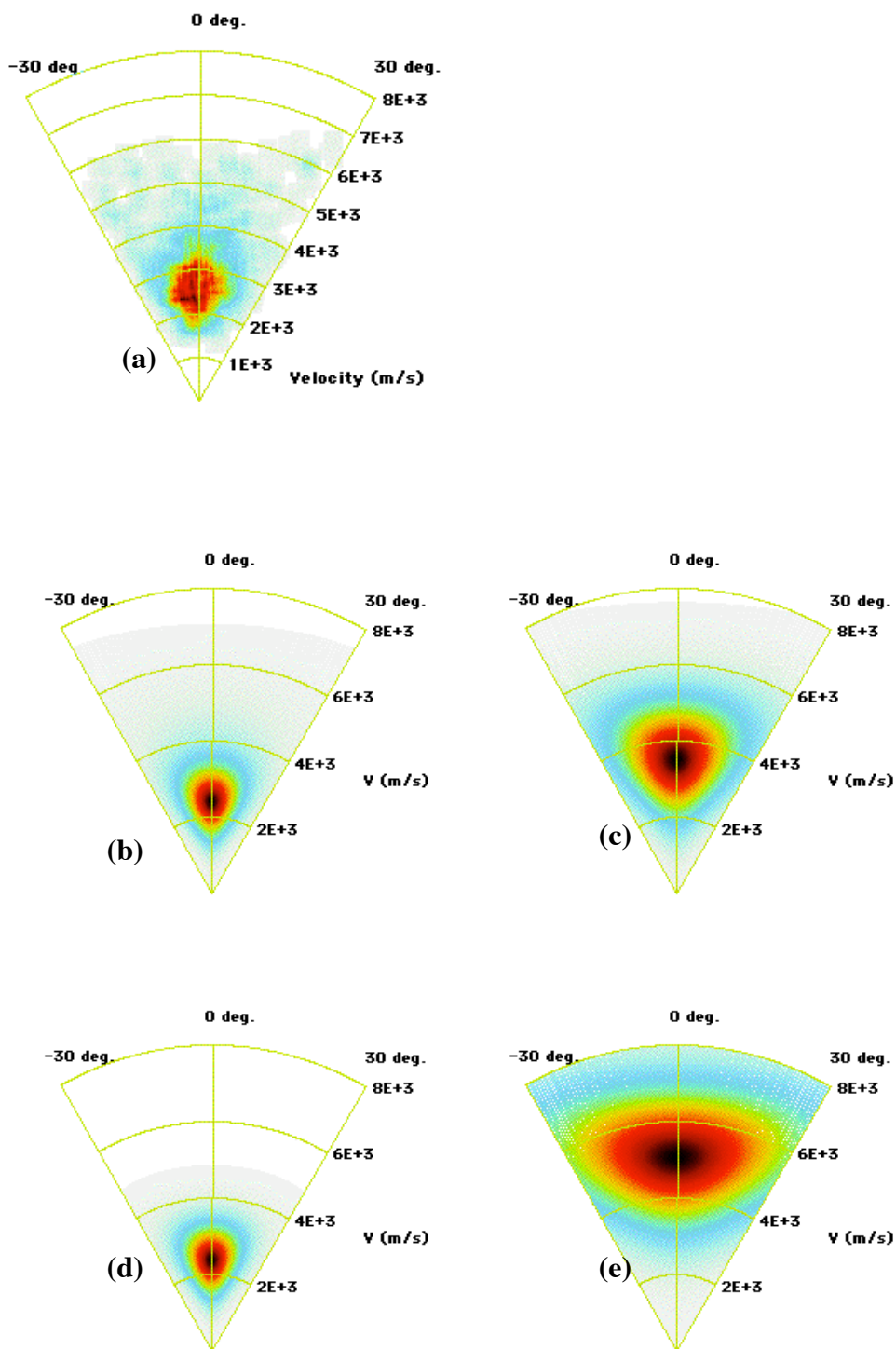


Figure A.4.8. Comparison of the parameterized fits to the experimental data for the  $\text{Br}^-(^1S_0)$  product intensity versus polar exit velocity at 74 eV incident energy. (a) Experimental data and (b) parameterized fit all three components combined, (c)  $\bar{\sigma}$  component only, (d)  $\bar{\sigma}$  component only, and (e)  $\bar{\sigma}$  component only. Red indicates the highest product yield and white indicates the lowest intensity.

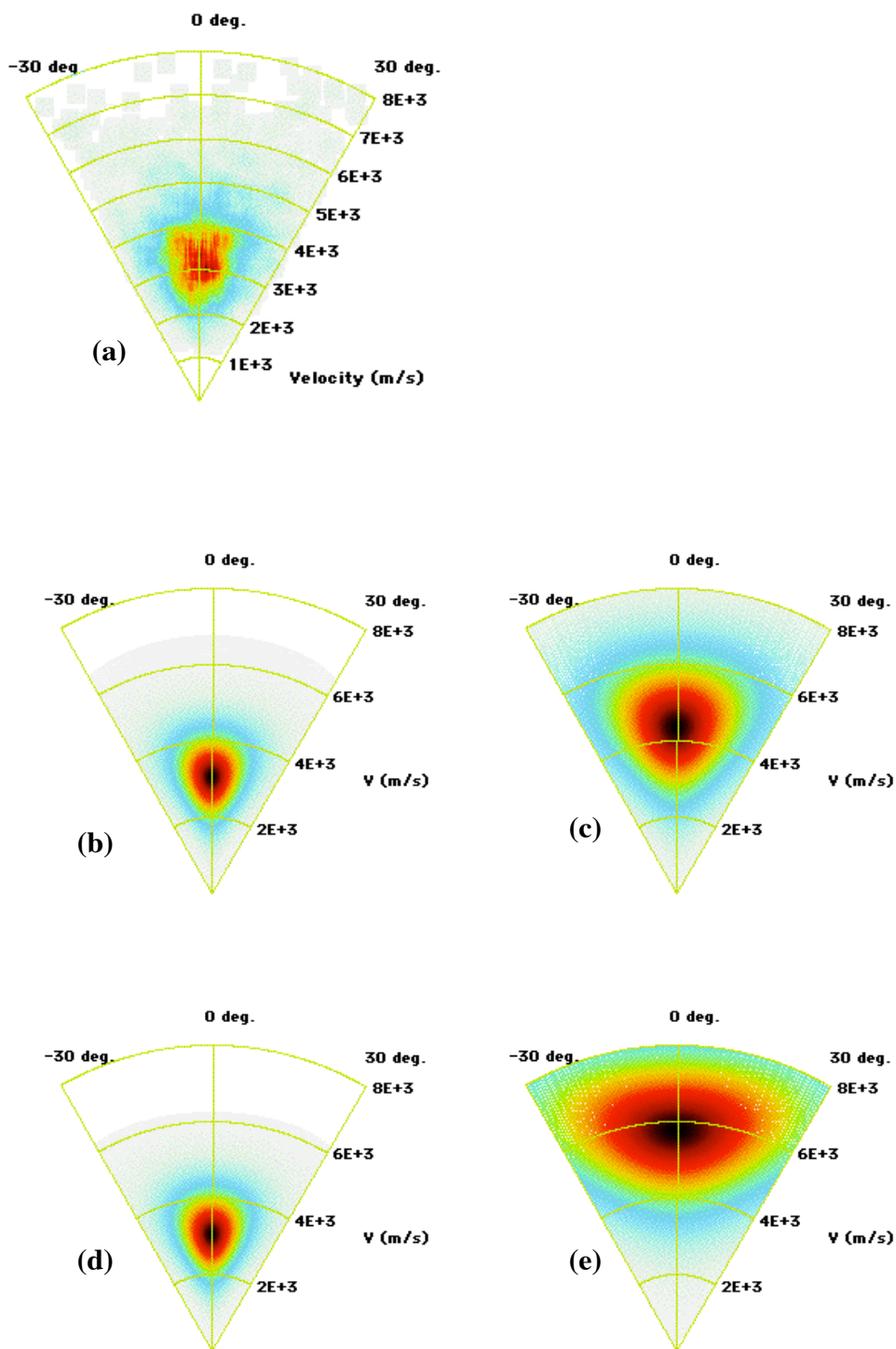


Figure A.4.9. Comparison of the parameterized fits to the experimental data for the  $\text{Br}^-(^1S_0)$  product intensity versus polar exit velocity at 94 eV incident energy. (a) Experimental data and (b) parameterized fit all three components combined, (c)  $\bar{\Gamma}$  component only, (d)  $\bar{\Gamma}$  component only, and (e)  $\bar{\Gamma}$  component only. Red indicates the highest product yield and white indicates the lowest intensity.



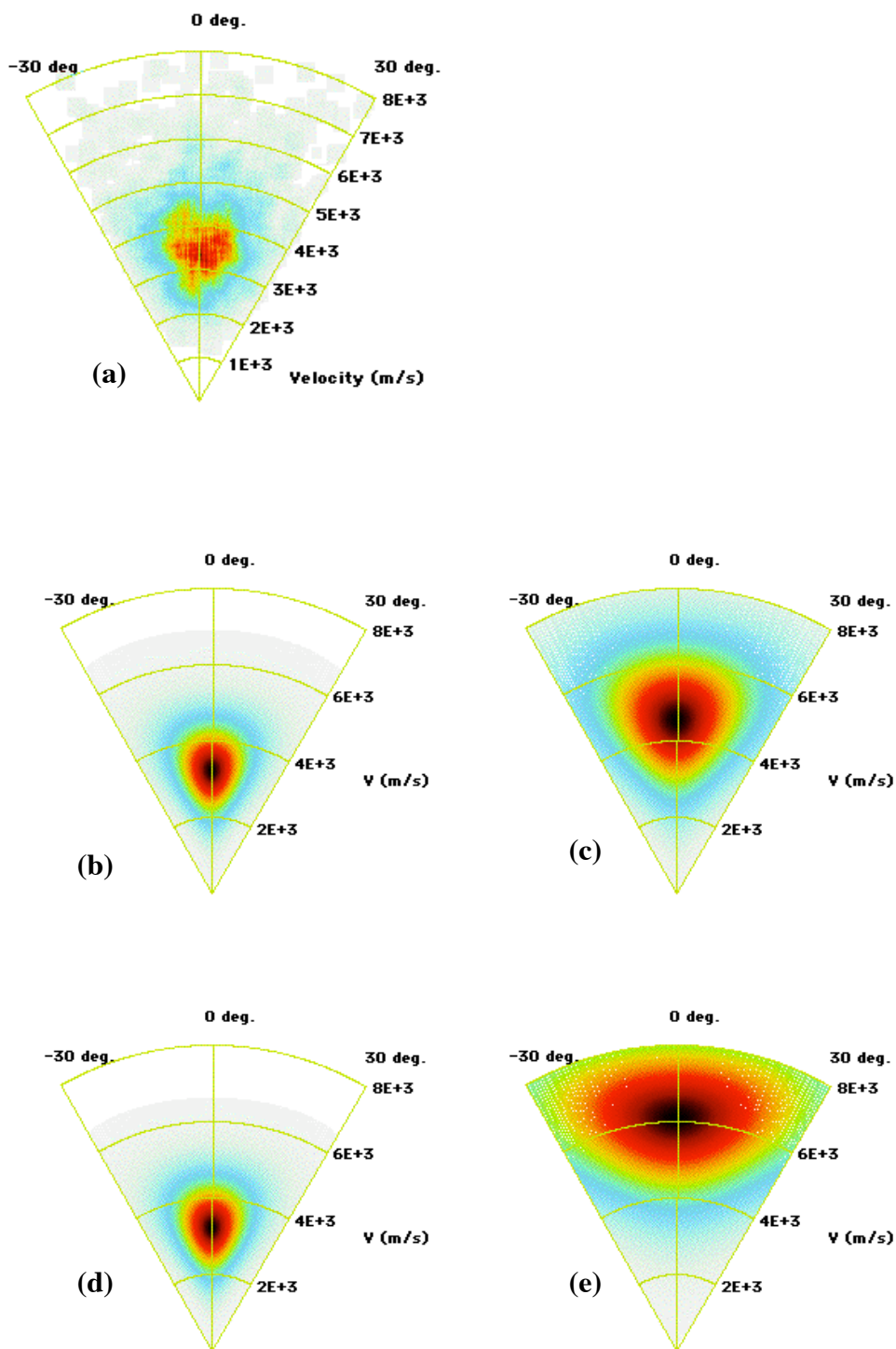


Figure A.4.10. Comparison of the parameterized fits to the experimental data for the  $\text{Br}^-(^1S_0)$  product intensity versus polar exit velocity at 104 eV incident energy. (a) Experimental data and (b) parameterized fit all three components combined, (c)  $\bar{\gamma}$  component only, (d)  $\bar{\gamma}$  component only, and (e)  $\bar{\gamma}$  component only. Red indicates the highest product yield and white indicates the lowest intensity.

### A.5. Br<sup>+</sup> Curve Fits at T<sub>s</sub> = 400° C

The following graphs represent the results from a series of curve fits to Br<sup>-</sup> product velocity-, polar- intensity, and polar energy- distributions described in Sect. 3.3.2 for Br<sup>+</sup> scattered on Pt(111) at 400° C across the 14 eV – 104 eV incident energy range. Briefly, the velocity distributions shown in Figures A.3.1-A.3.13 (a) are fit to a series of three Gaussian functions,  $\square$ ,  $\square$ , and  $\square$  according to equation 3.2. For the polar intensity plots in Figures A.3.1-A.3.13 (b), the  $\square$ ,  $\square$ , and  $\square$  components are calculated according to equation 3.6 with the width parameter,  $n_i$ , for each component held constant across the incident energy range. The polar energy curve fits are calculated from the polar intensity fits and the average energy values obtained from the velocity distribution fits.

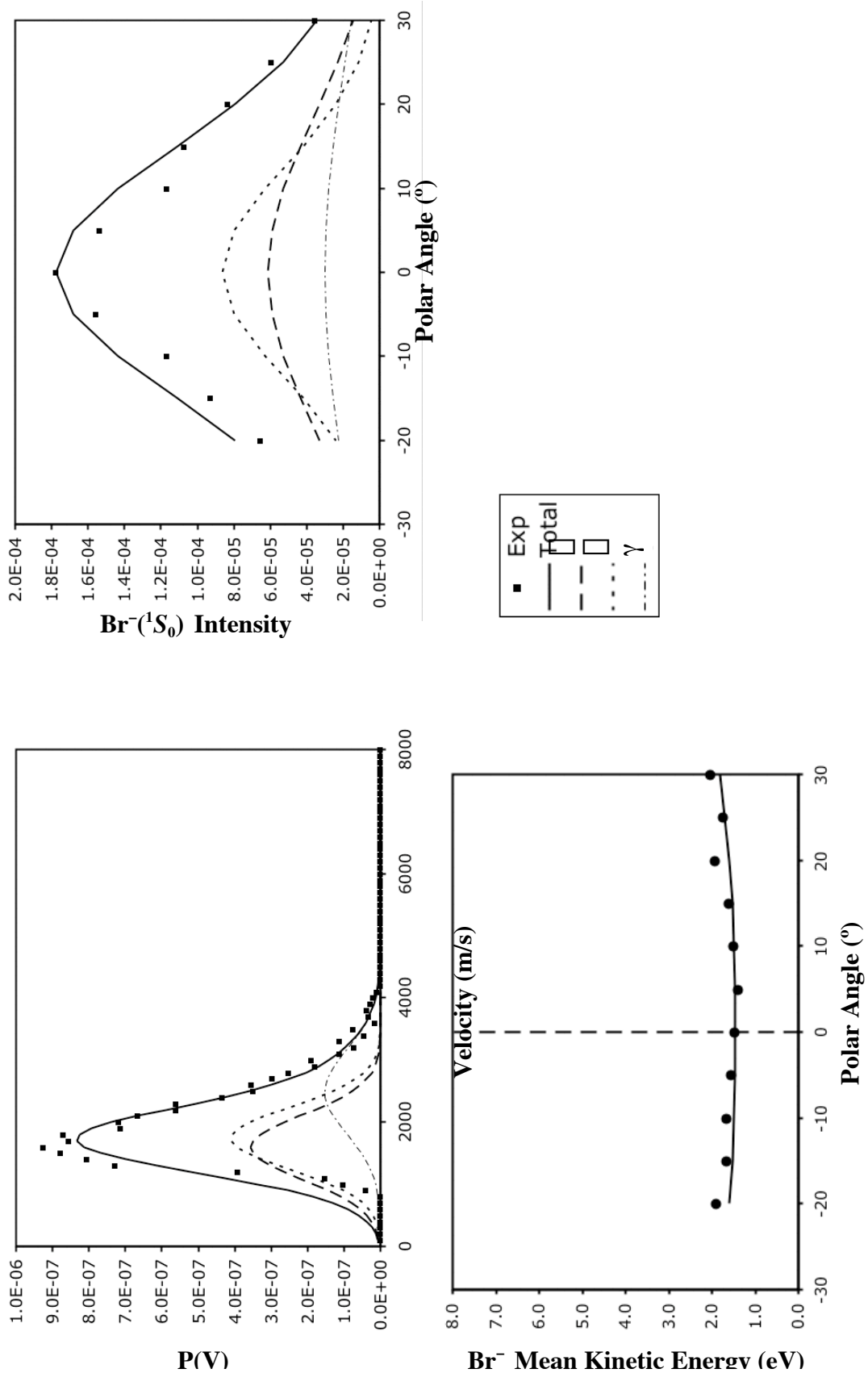


Figure A.5.1. Br<sup>-</sup>(<sup>1</sup>S<sub>0</sub>) (a) product velocity distributions (b) polar intensity distribution and (c) polar energy distribution for 14 eV incident Br<sup>+</sup>(<sup>3</sup>P<sub>2</sub>) collision energy on Pt(111) at T<sub>s</sub> = 400° C. The  $\square$ ,  $\square$ , and  $\square$  components are calculated according to equations 3.2 and 3.6. The solid lines that represent the sum of the three components is compared to the data in each plot.

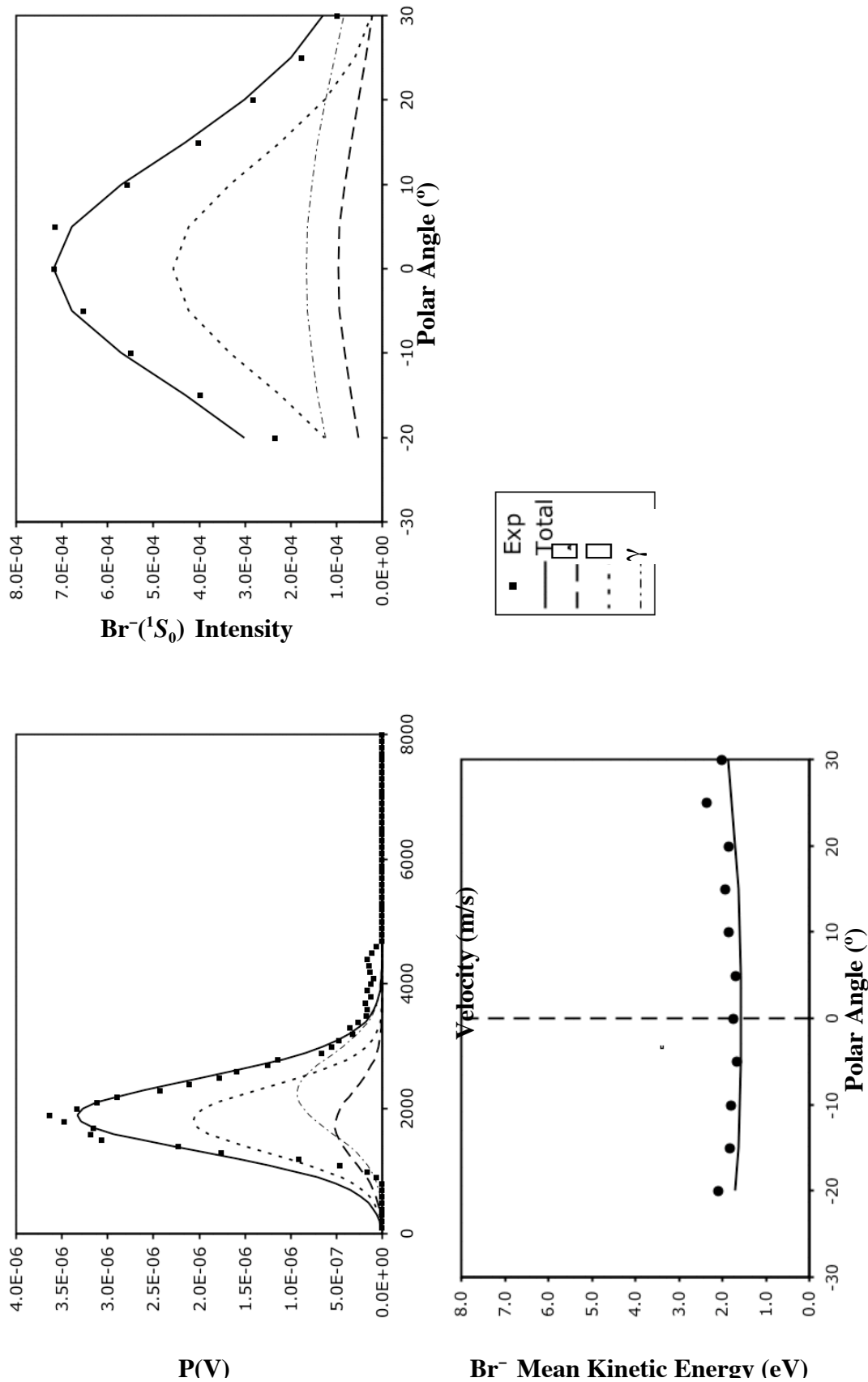


Figure A.5.2.  $\text{Br}^-(^1S_0)$  (a) product velocity distributions (b) polar intensity distribution and (c) polar energy distribution for 19 eV incident  $\text{Br}^+(^3P_2)$  collision energy on Pt(111) at  $T_s = 400^\circ\text{C}$ . The  $\square$ ,  $\square$ , and  $\square$  components are calculated according to equations 3.2 and 3.6. The solid lines that represent the sum of the three components is compared to the data in each plot.

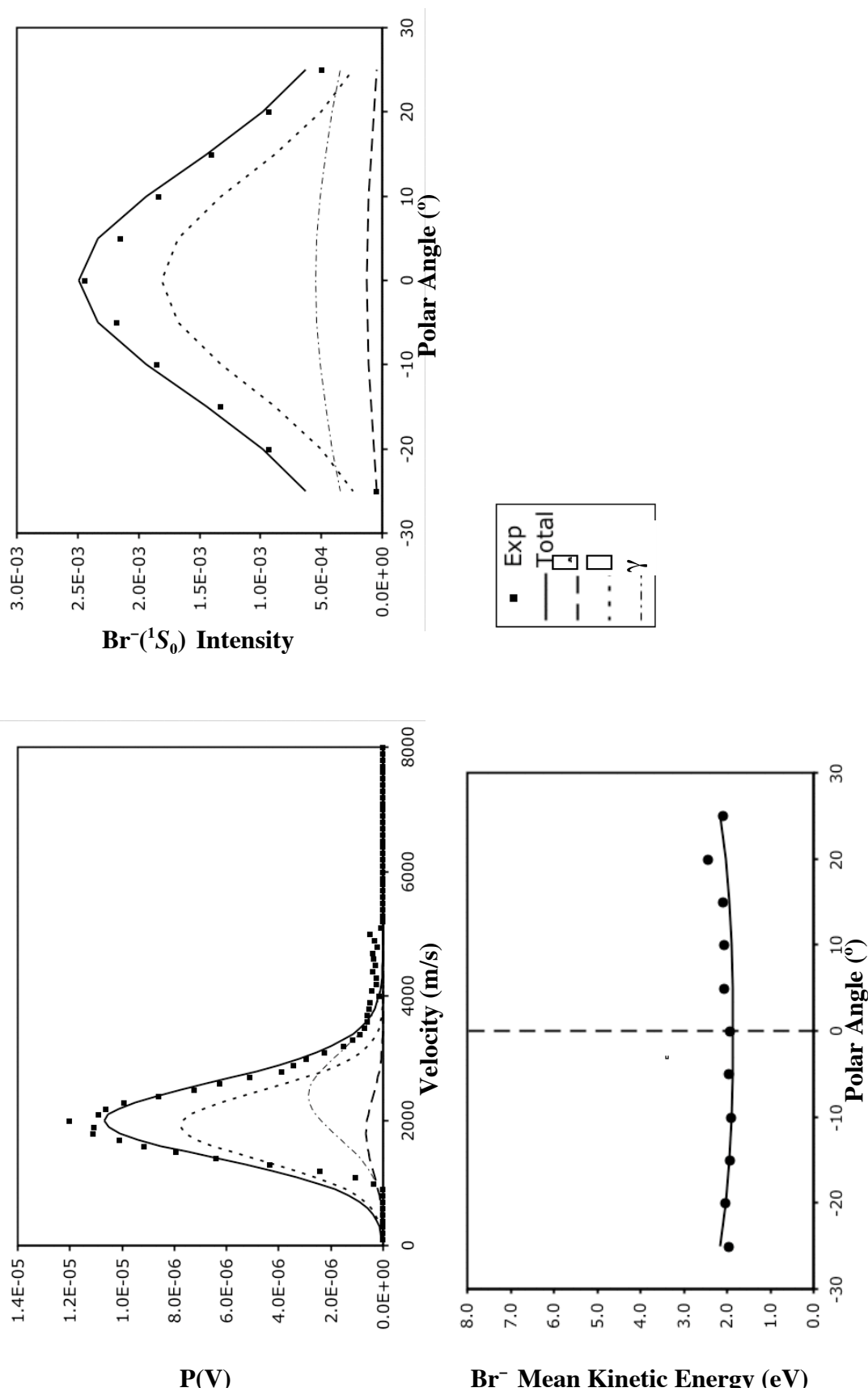


Figure A.5.3.  $\text{Br}^-(^1S_0)$  (a) product velocity distributions (b) polar intensity distribution and (c) polar energy distribution for 21.5 eV incident  $\text{Br}^+(^3P_2)$  collision energy on Pt(111) at  $T_s = 400^\circ \text{C}$ . The  $\square$ ,  $\diamond$ , and  $\gamma$  components are calculated according to equations 3.2 and 3.6. The solid lines that represent the sum of the three components is compared to the data in each plot.

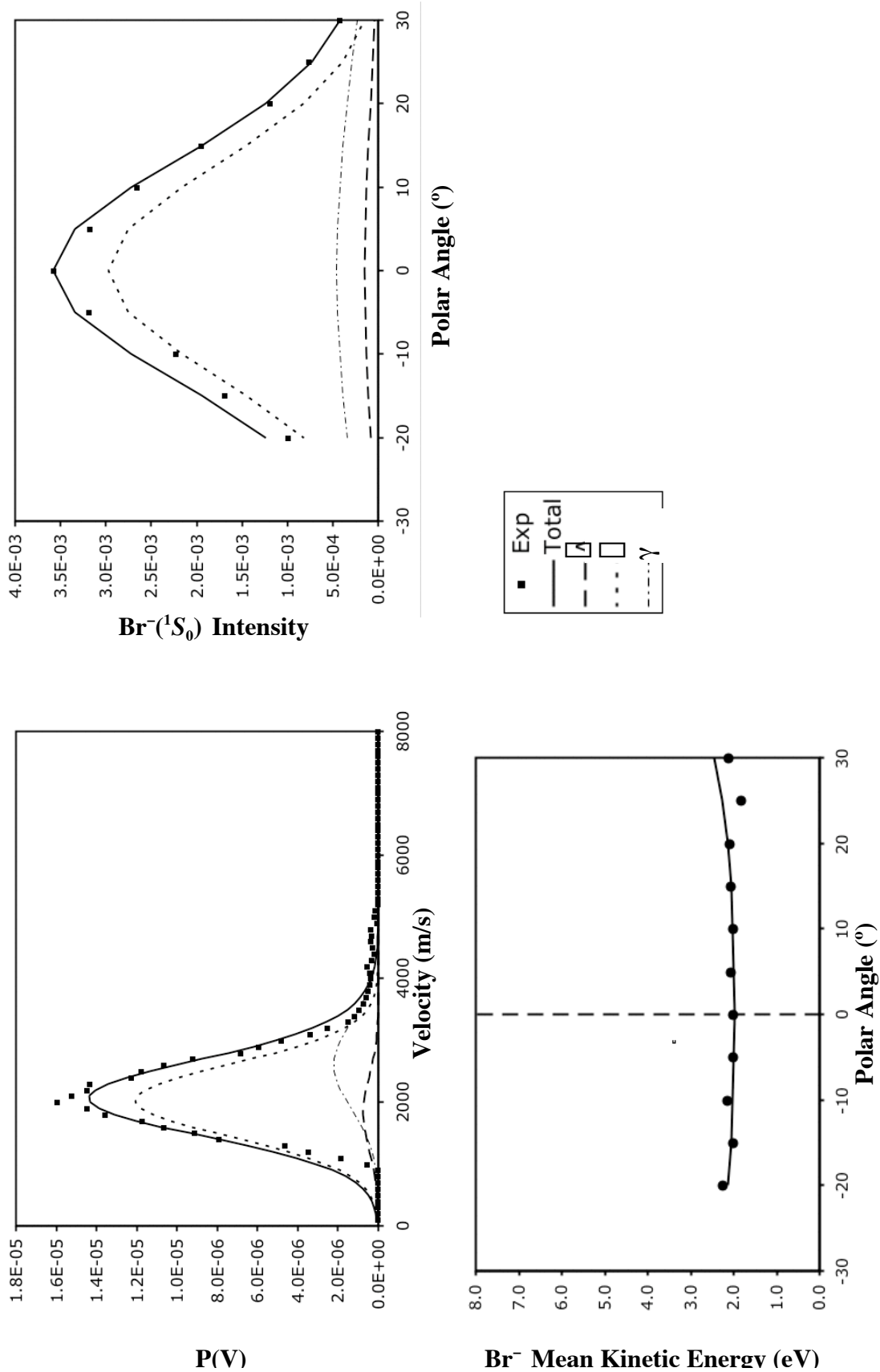


Figure A.5.4.  $\text{Br}^+(^1S_0)$  (a) product velocity distributions (b) polar intensity distribution and (c) polar energy distribution for 24 eV incident  $\text{Br}^+(^3P_2)$  collision energy on Pt(111) at  $T_s = 400^\circ\text{C}$ . The  $\square$ ,  $\square'$ ,  $\square''$ , and  $\square'''$  components are calculated according to equations 3.2 and 3.6. The solid lines that represent the sum of the three components is compared to the data in each plot.

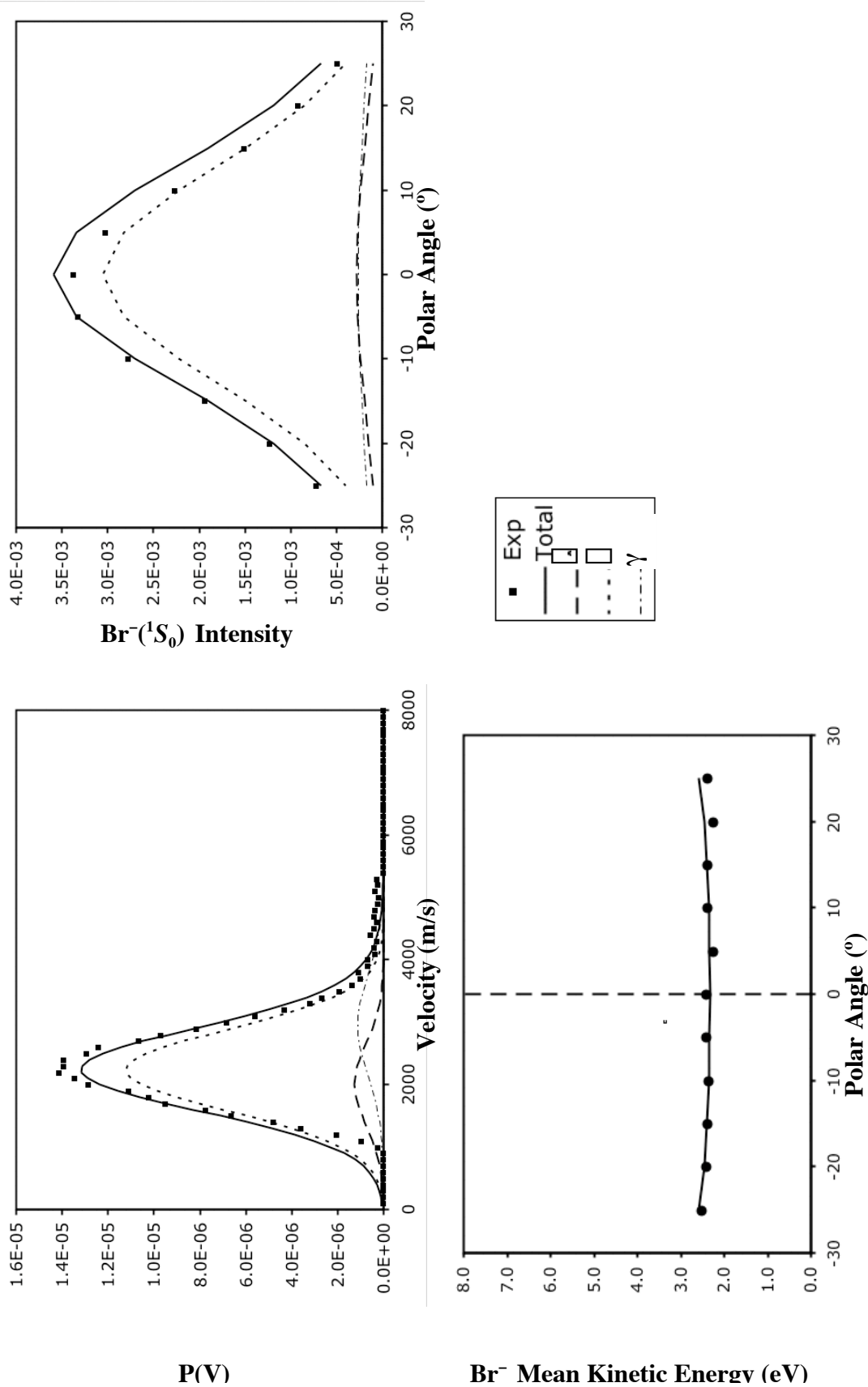


Figure A.5.5.  $\text{Br}^-(^1S_0)$  (a) product velocity distributions (b) polar intensity distribution and (c) polar energy distribution for 29 eV incident  $\text{Br}^+(^3P_2)$  collision energy on Pt(111) at  $T_s = 400^\circ \text{C}$ . The  $\square$ ,  $\square$ , and  $\gamma$  components are calculated according to equations 3.2 and 3.6. The solid lines that represent the sum of the three components is compared to the data in each plot.

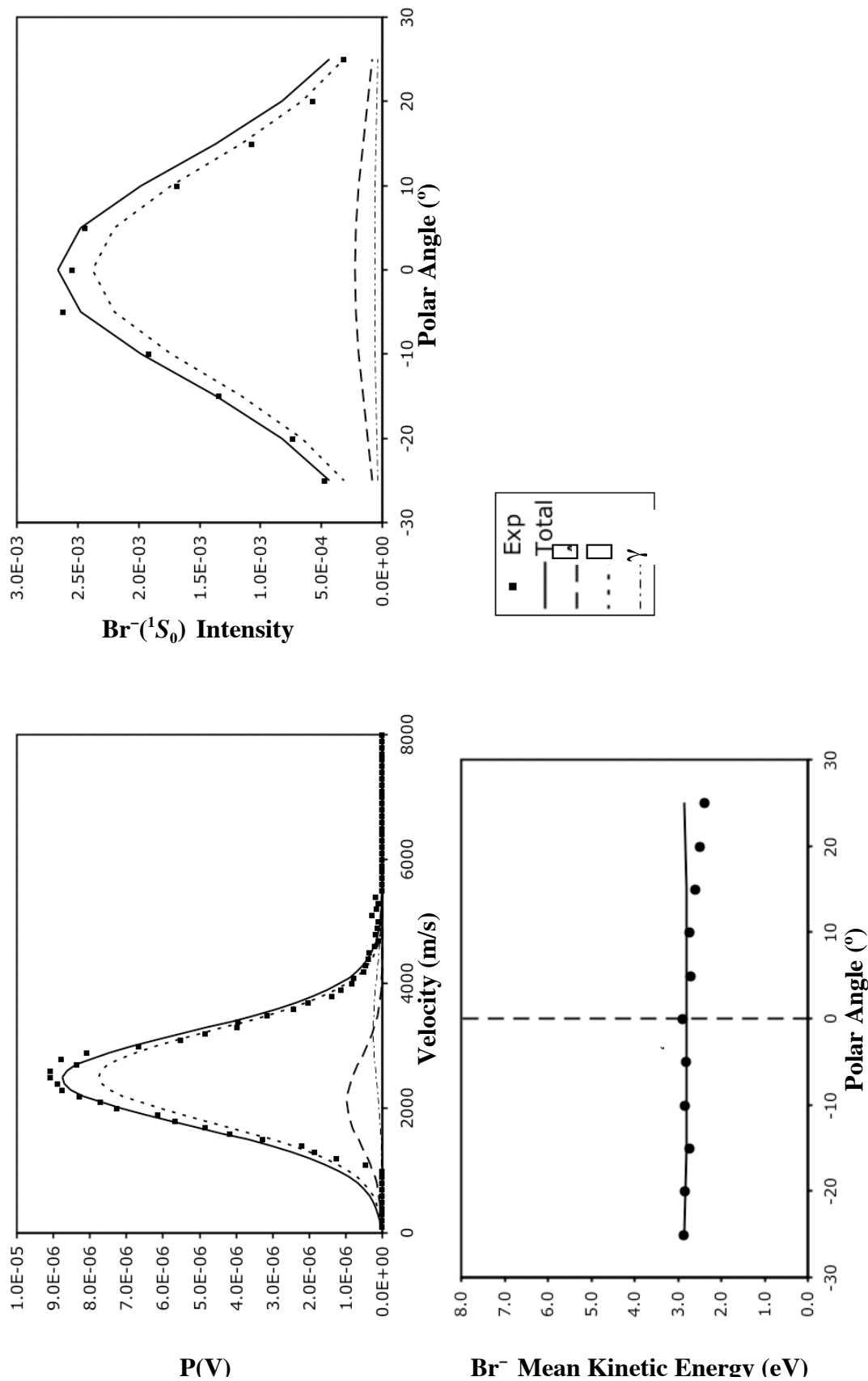


Figure A.5.6.  $\text{Br}^-(^1S_0)$  (a) product velocity distributions (b) polar intensity distribution and (c) polar energy distribution for 34 eV incident  $\text{Br}^+(^3P_2)$  collision energy on Pt(111) at  $T_s = 400^\circ\text{C}$ . The  $\square$ ,  $\square$ , and  $\square$  components are calculated according to equations 3.2 and 3.6. The solid lines that represent the sum of the three components is compared to the data in each plot.



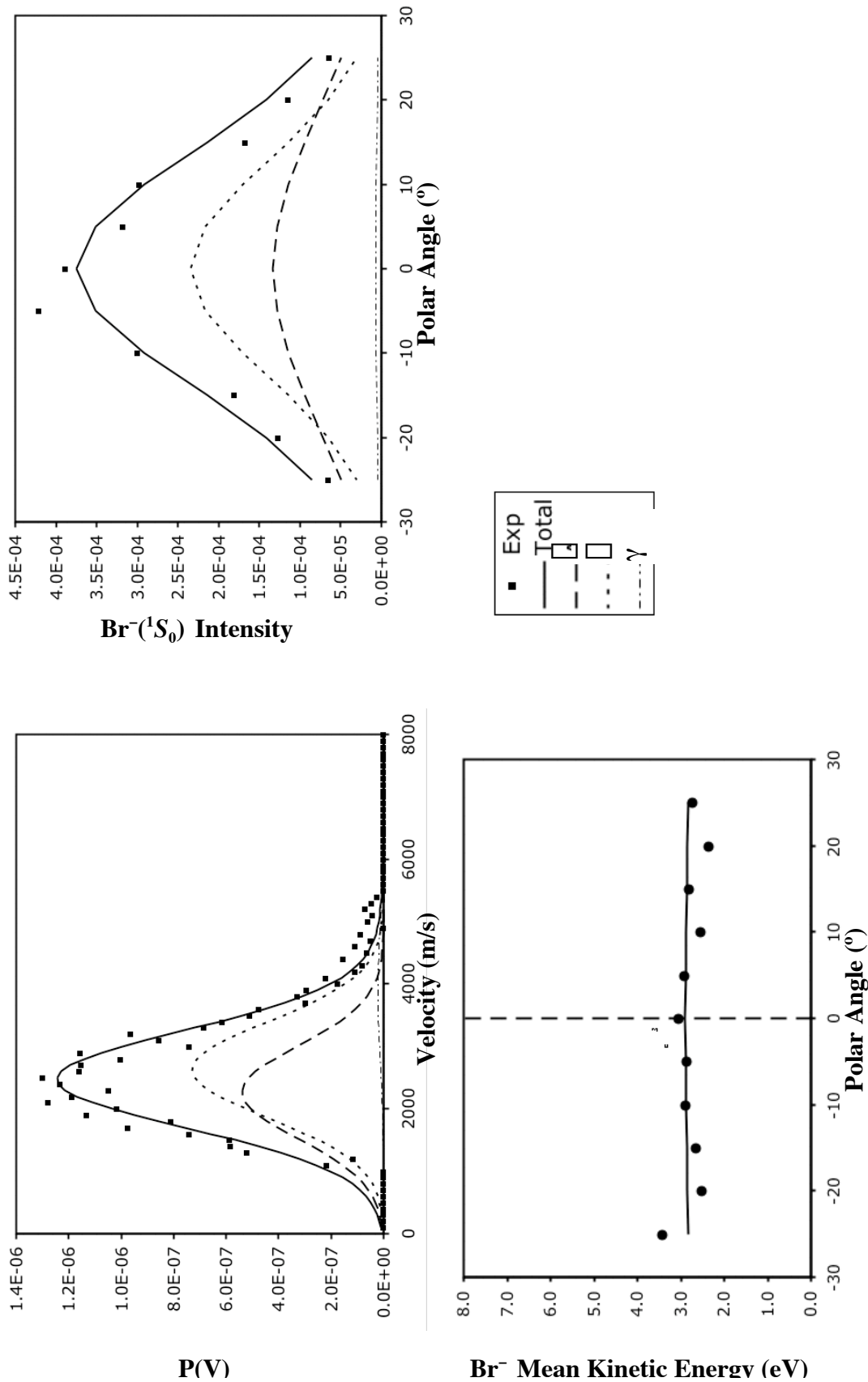


Figure A.5.7. Br<sup>-</sup>(<sup>1</sup>S<sub>0</sub>) (a) product velocity distributions (b) polar intensity distribution and (c) polar energy distribution for 44 eV incident Br<sup>+</sup>(<sup>3</sup>P<sub>2</sub>) collision energy on Pt(111) at T<sub>s</sub> = 400° C. The  $\square$ ,  $\square$ , and  $\square$  components are calculated according to equations 3.2 and 3.6. The solid lines that represent the sum of the three components is compared to the data in each plot.

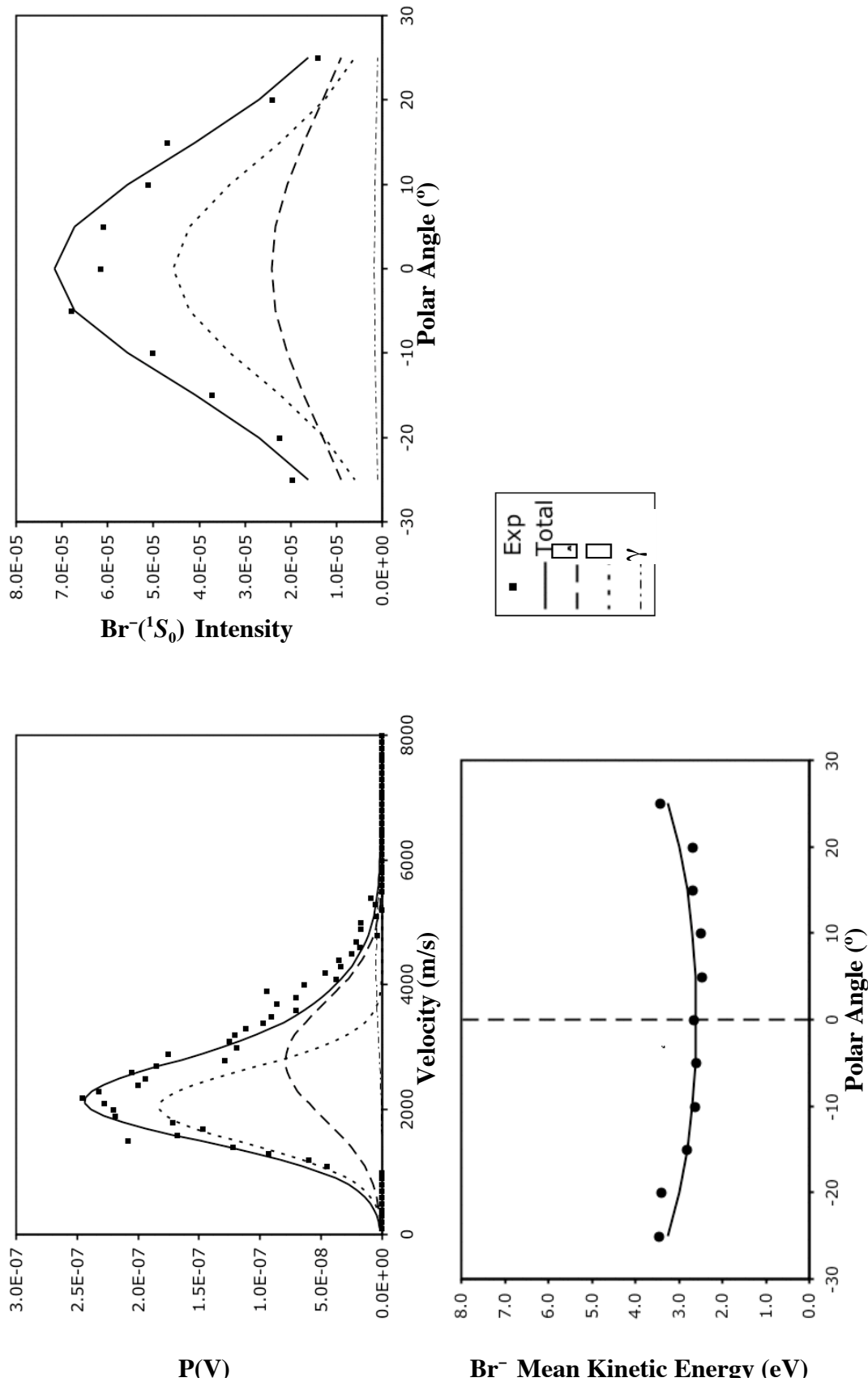


Figure A.5.8.  $\text{Br}^-(^1S_0)$  (a) product velocity distributions (b) polar intensity distribution and (c) polar energy distribution for 54 eV incident  $\text{Br}^+(^3P_2)$  collision energy on Pt(111) at  $T_s = 400^\circ\text{C}$ . The  $\square$ ,  $\square$ , and  $\square$  components are calculated according to equations 3.2 and 3.6. The solid lines that represent the sum of the three components is compared to the data in each plot.

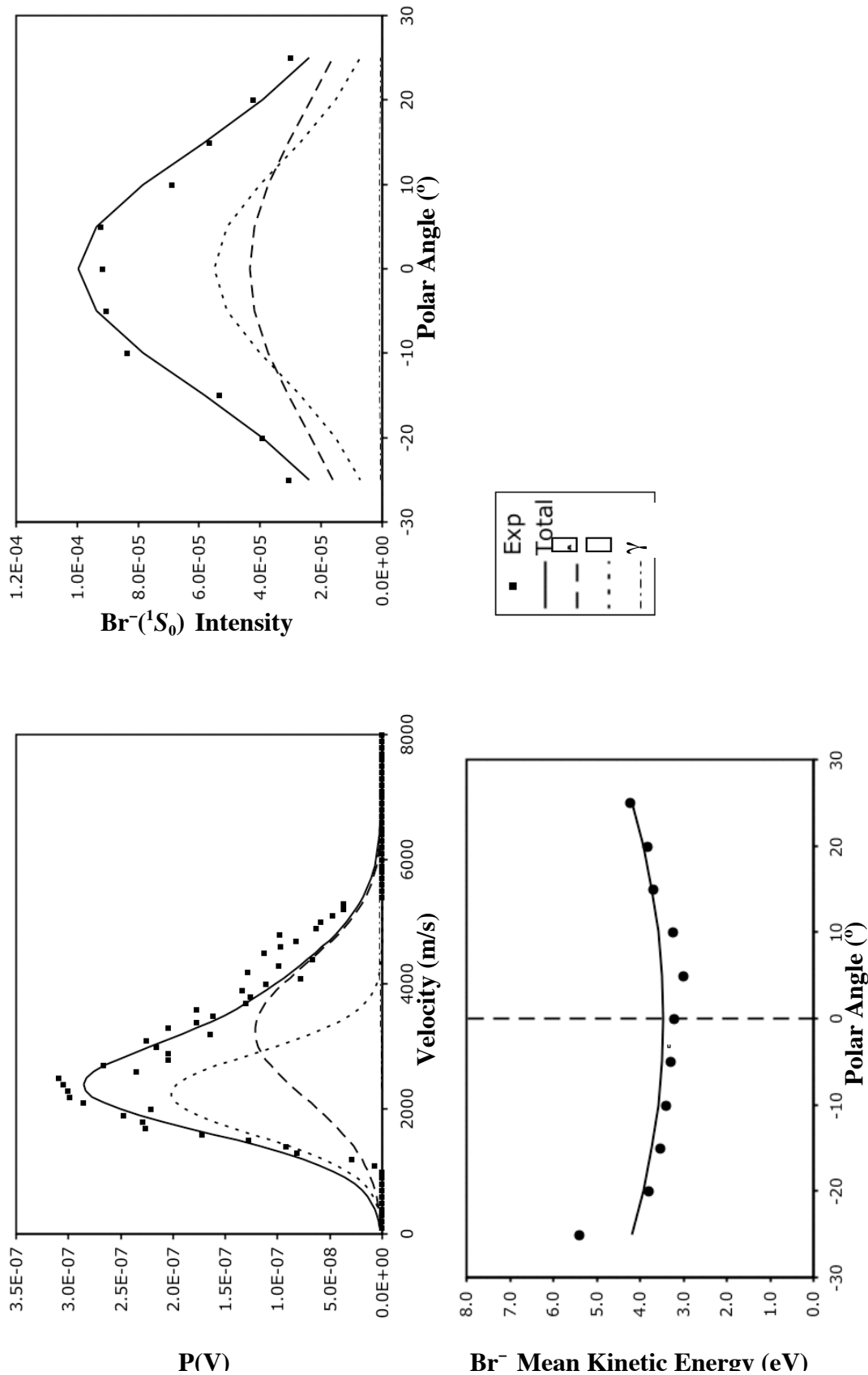


Figure A.5.9.  $\text{Br}^-(^1S_0)$  (a) product velocity distributions (b) polar intensity distribution and (c) polar energy distribution for 64 eV incident  $\text{Br}^+(^3P_2)$  collision energy on Pt(111) at  $T_s = 400^\circ\text{C}$ . The  $P$ ,  $D$ , and  $\gamma$  components are calculated according to equations 3.2 and 3.6. The solid lines that represent the sum of the three components is compared to the data in each plot.

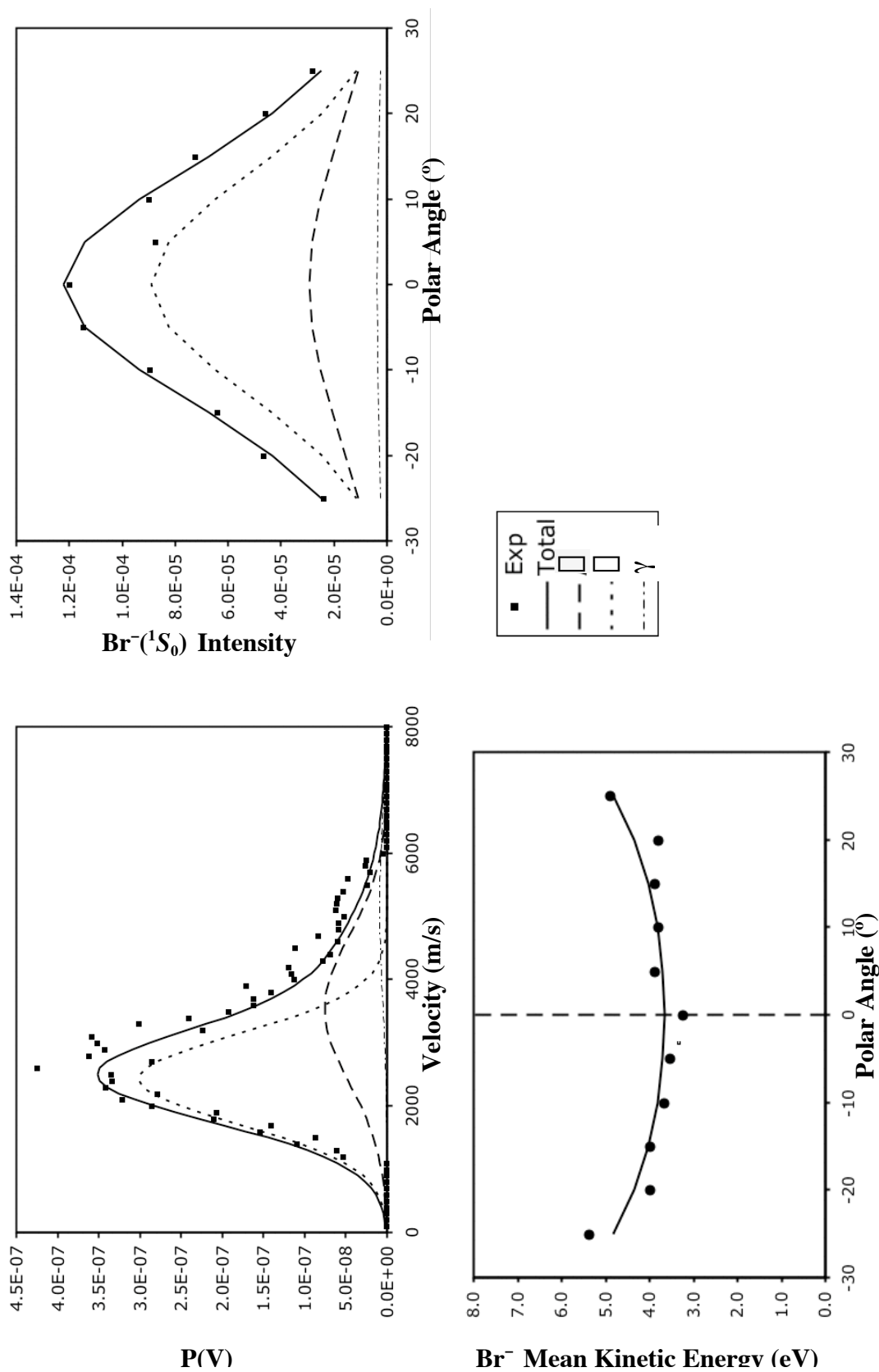


Figure A.5.10.  $Br^{-}(^1S_0)$  (a) product velocity distributions (b) polar intensity distribution and (c) polar energy distribution for 74 eV incident  $Br^{+}(^3P_2)$  collision energy on Pt(111) at  $T_s = 400^{\circ}C$ . The  $\square$ ,  $\square$ , and  $\square$  components are calculated according to equations 3.2 and 3.6. The solid lines that represent the sum of the three components is compared to the data in each plot.

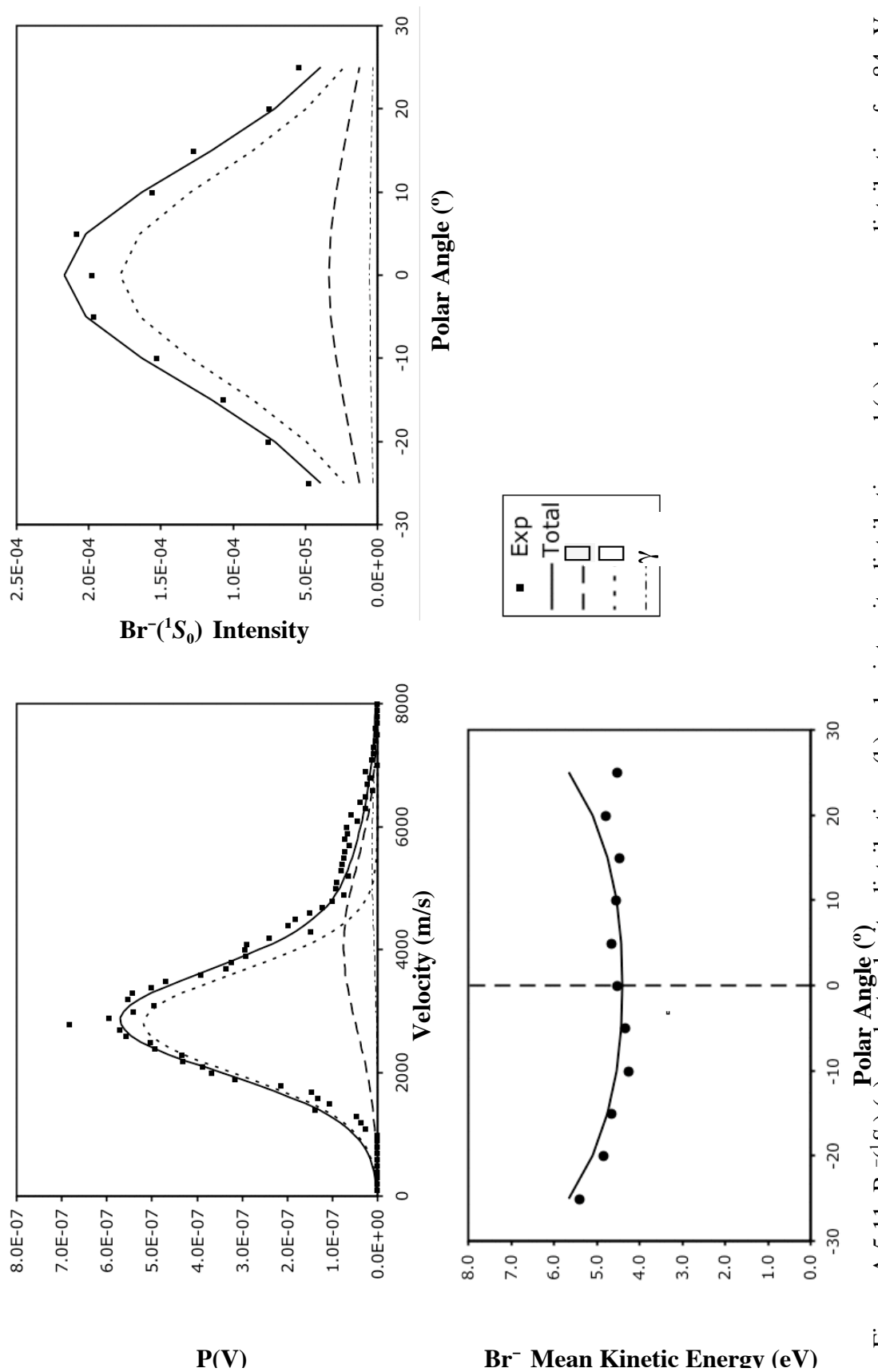


Figure A.5.11.  $\text{Br}^-(^1S_0)$  (a) product velocity distributions (b) polar intensity distribution and (c) polar energy distribution for 84 eV incident  $\text{Br}^+(^3P_2)$  collision energy on Pt(111) at  $T_s = 400^\circ\text{C}$ . The  $\square$ ,  $\square$ , and  $\square$  components are calculated according to equations 3.2 and 3.6. The solid lines that represent the sum of the three components is compared to the data in each plot.

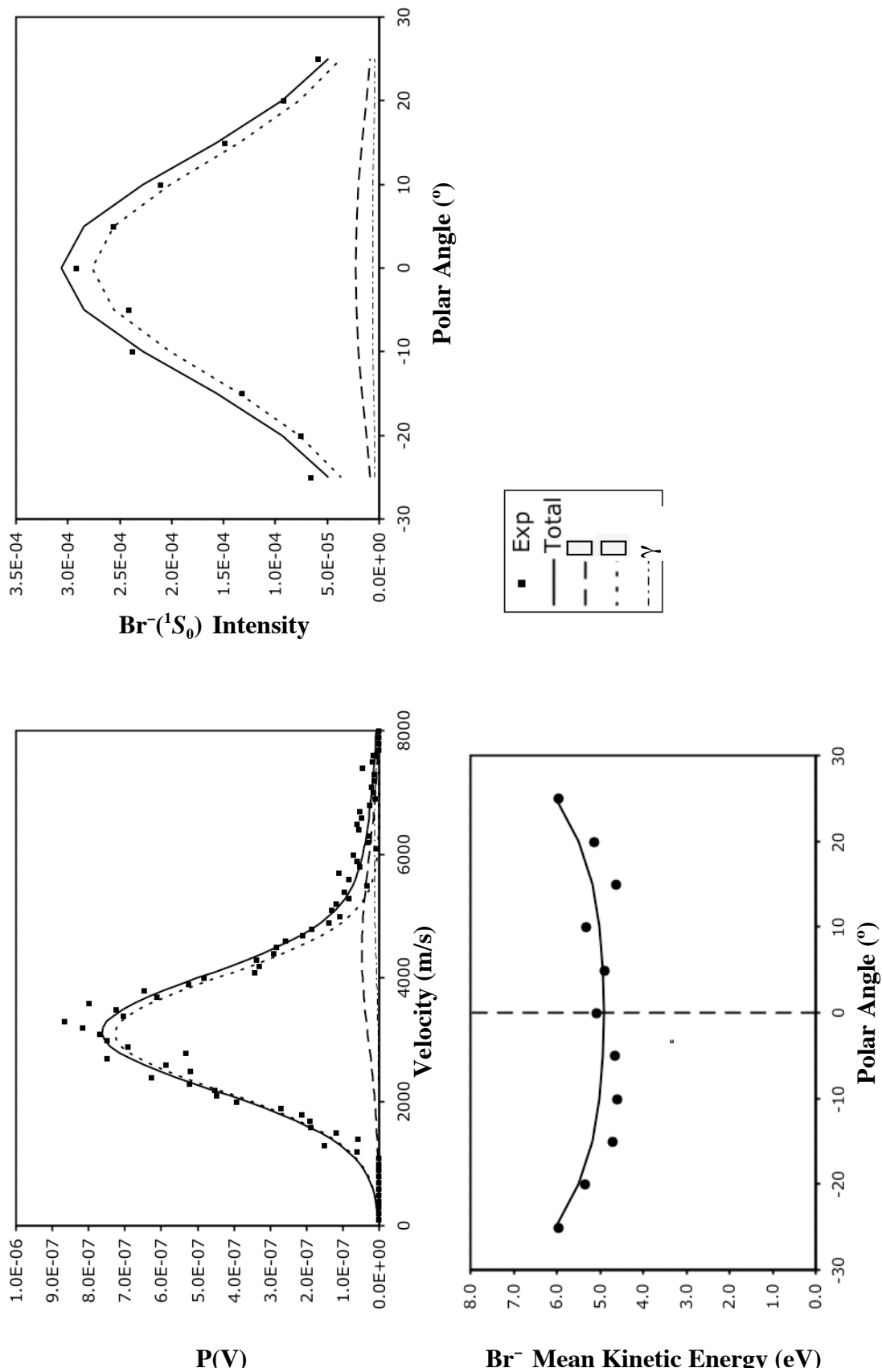


Figure A.5.12.  $\text{Br}^-({}^1S_0)$  (a) product velocity distributions (b) polar intensity distribution and (c) polar energy distribution for 94 eV incident  $\text{Br}^+({}^3P_2)$  collision energy on Pt(111) at  $T_s = 400^\circ \text{C}$ . The  $\square$ ,  $\square$ , and  $\square$  components are calculated according to equations 3.2 and 3.6. The solid lines that represent the sum of the three components is compared to the data in each plot.

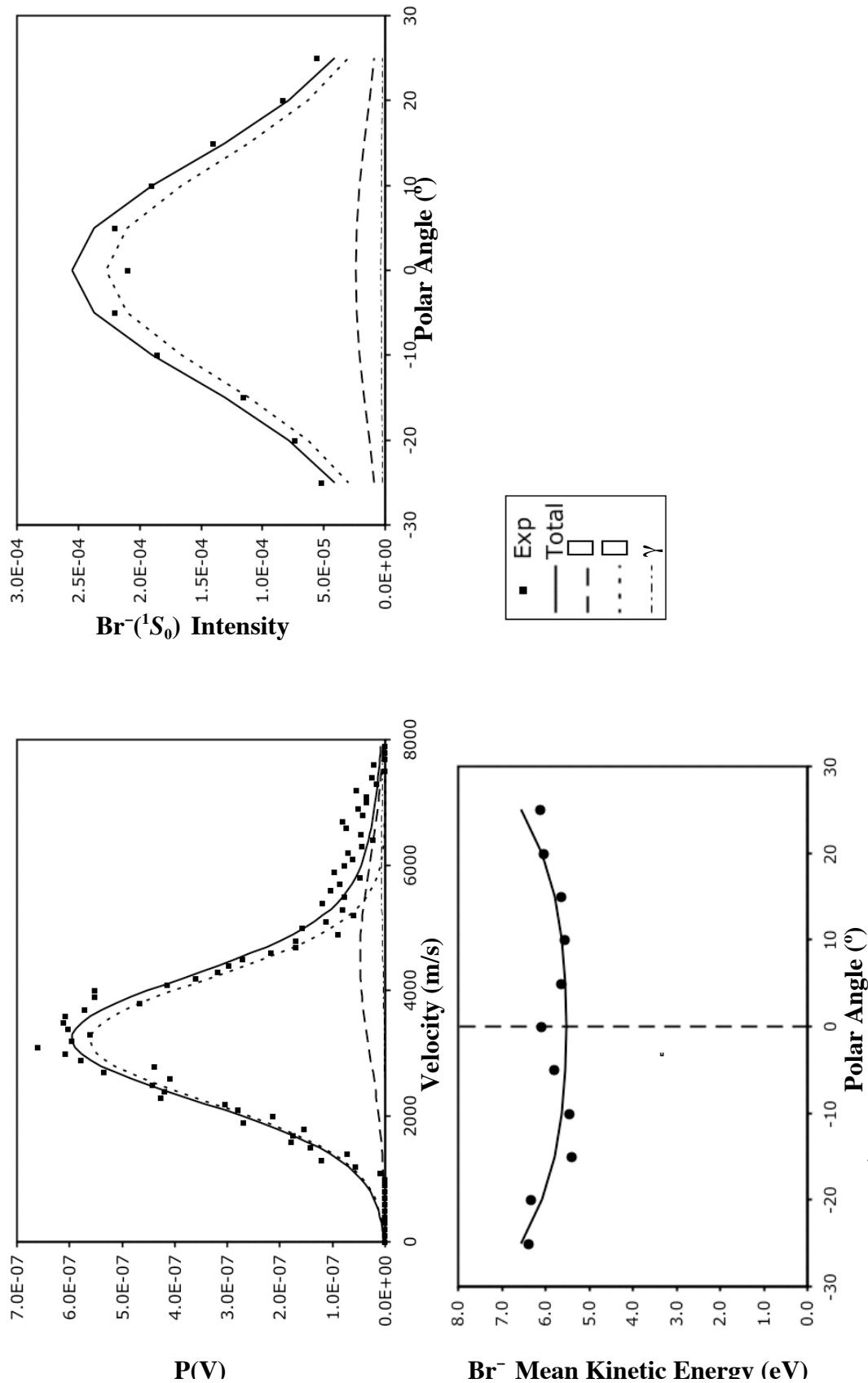


Figure A.5.13.  $\text{Br}^-(\text{}^1S_0)$  (a) product velocity distributions (b) polar intensity distribution and (c) polar energy distribution for 104 eV incident  $\text{Br}^+(\text{}^3P_2)$  collision energy on Pt(111) at  $T_s = 400^\circ\text{C}$ . The  $\square$ ,  $\square$ , and  $\square$  components are calculated according to equations 3.2 and 3.6. The solid lines that represent the sum of the three components is compared to the data in each plot.

## REFERENCES

- Adler, D. L. and Cooper, B. H. (1991) *Physical Review B*, **43**, 3876-3892.
- Akazawa, H. and Murata, Y. (1990) *Journal of Chemical Physics*, **92**, 5560-5568.
- Amirav, A., Cardillo, M. J., Trevor, P. L., Lim, C. and Tully, J. C. (1987) *Journal of Chemical Physics*, **87**, 1796-1807.
- Andersen, E. and Simons, J. (1977) *Journal of Chemical Physics*, **66**, 2427-2430.
- Anderson, S. L. (1992) *Advances in Chemical Physics*, **82**, 177-212.
- Aono, M. (1984) *Nuclear Instruments & Methods in Physics Research Section B-Beam Interactions with Materials and Atoms*, **230**, 374-383.
- Asscher, M., Guthrie, W. L., Lin, T.-H. and Somorjai, G. A. (1983) *Journal of Chemical Physics*, **78**, 6992-7004.
- Batra, I. P. and Kleinman, L. (1984) *Journal of Electron Spectroscopy and Related Phenomena*, **33**, 175-241.
- Behringer, E. R., Andersson, D. R., Cooper, B. H. and Marston, J. B. (1996) *Physical Review B*, **54**, 14765-14779.
- Bekkerman, A., Tsipinyuk, B. and Kolodney, E. (2000) *Physical Review B*, **61**, 10463-10470.
- Bekkerman, A., Tsipinyuk, B. and Kolodney, E. (2002) *Journal of Chemical Physics*, **116**, 10447-10457.
- Borisov, A. G. and Esaulov, V. A. (2000) *Journal of Physics-Condensed Matter*, **12**, R177-R206.
- Borisov, A. G., Teillet-Billy, D., Gauyacq, J. P., Silva, J. A. M. C., Mertens, A., Auth, C. and Winter, H. (1999) *Physical Review B*, **59**, 8218-8231.
- Brako, R. and Newns, D. (1989) *Rep. Prog. Phys.*, **52**, 655.
- Brako, R. and Newns, D. M. (1981) *Surface Science*, **108**, 253-270.



- Brune, H., Wintterlin, J., Trost, J., Ertl, G., Wiechers, J. and Behm, R. J. (1993) *Journal of Chemical Physics*, **99**, 2128-2148.
- Bu, Y., Greene, E. F. and Stewart, D. K. (1990) *Journal of Chemical Physics*, **92**, 3899-3908.
- Buntin, S. A. (1998) *Journal of Chemical Physics*, **108**, 1601-1609.
- Chandezon, F., Huber, B. and Ristori, C. (1994) *Review of Scientific Instruments*, **65**, 3344-3353.
- Chen, E. S. and Chen, E. C. M. (2003) *Journal of Physical Chemistry A*, **107**, 169-177.
- Childs, K. D., Carlson, B. A., LaVanier, L. A., Moulder, J. F., Paul, D. F., Stickle, W. F. and Watson, D. G. (1995) *Handbook of Auger Electron Spectroscopy*, Physical Electronics, Inc, Eden Prairie, MN.
- Christmann, K., Ertl, G. and Pignet, T. (1976) *Surface Science*, **54**, 365-392.
- Chuang, T. J., Schwarzwald, R. and Modl, A. (1991) *Journal of Vacuum Science & Technology a-Vacuum Surfaces and Films*, **9**, 1719-1725.
- Cooper, B. H. and Behringer, E. R. (1994) In *Low Energy Ion-Surface Interactions, Advances in Ion Chemistry and Physics*(Ed, Rabalais, J. W.) John Wiley & Sons, Sussex.
- Corr, D. and Jacobs, D. C. (1992) *Review of Scientific Instruments*, **63**, 1969-1972.
- Dahl, D. A. (1995) Idaho National Engineering Laboratory, Idaho Falls, ID.
- Darko, T., Baldwin, D. A., Shamir, N., Rabalais, J. W. and Hochmann, P. (1982) *Journal of Chemical Physics*, **76**, 6408-6416.
- Darling, G. R. and Holloway, S. (1995) *Reports on Progress in Physics*, **58**, 1595-1672.
- DiRubio, C. A., McEachern, R. L., McLean, J. G. and Cooper, B. H. (1996) *Physical Review B*, **54**, 8862-8881.
- Fraser, G. W. (2002) *International Journal of Mass Spectrometry*, **215**, 13-30.
- Gauyacq, J. P. and Borisov, A. G. (1998) *Journal of Physics-Condensed Matter*, **10**, 6585-6619.

- German, K. A. H., Weare, C. B., Varekamp, P. R., Andersen, J. N. and Yarmoff, J. A. (1993) *Physical Review Letters*, **70**, 3510-3513.
- Goodman, F. O. and Sulston, K. W. (2001) *Journal of Chemical Physics*, **114**, 3265-3270.
- Greeley, J. N. (1995) In *Department of Chemistry and Biochemistry* University of Notre Dame, Notre Dame.
- Greeley, J. N., Martin, J. S., Morris, J. R. and Jacobs, D. C. (1994) *Surface Science*, **314**, 97-106.
- Greeley, J. N., Martin, J. S., Morris, J. R. and Jacobs, D. C. (1995) *Journal of Chemical Physics*, **102**, 4996-5011.
- Grill, V., Shen, J., Evans, C. and Cooks, R. G. (2001) *Review of Scientific Instruments*, **72**, 3149-3179.
- Han, S.-J., Lee, C.-W., Lahaye, R. J. W. E. and Kang, H. (2003) *Surface Science*, **538**, 184-190.
- Hoek, P. J. v. d. and Kleyn, A. W. (1989) *Journal of Chemical Physics*, **91**, 4318-4329.
- Hoffman, A., Maniv, T. and Folman, M. (1987) *Surface Science*, **183**, 484-502.
- Huber, B. A., Cosby, P. C., Peterson, J. R. and Moseley, J. T. (1977) *Journal of Chemical Physics*, **66**, 4520-4526.
- Hulpke, E. and Mann, K. (1983) *Surface Science*, **133**, 171-198.
- Hwang, E., Dagdigian, P. J. and Tellinghuisen, J. (1997) *Journal of Molecular Spectroscopy*, **181**, 297-306.
- Jacobs, D. C. (2000) In *Chemical Dynamics in Extreme Environments* (Ed, Dressler, R.) World Sci., Singapore, pp. 349-389.
- Jacobs, D. C. (2002) *Annual Review of Physical Chemistry*, **53**, 379-407.
- Jacobsen, J., Hammer, B., Jacobsen, K. W. and Norskov, J. K. (1995) *Physical Review B*, **52**, 14954-14962.
- Jost, R., Nygard, J., Pasinski, A. and Delon, A. (1996) *Journal of Chemical Physics*, **105**, 1287-1290.
- Kaack, M. and Fick, D. (1995) *Surface Science*, **342**, 111-118.

- Kasi, S. R., Kang, H., Sass, C. S. and Rabalais, J. W. (1989) *Surface Science Reports*, **10**, 1-104.
- Kasi, S. R., Kilburn, M. A., Kang, H., Rabalais, J. W., Tavernini, L. and Hochmann, P. (1988) *Journal of Chemical Physics*, **88**, 5902-5913.
- Keller, C. A., Dirubio, C. A., Kimmel, G. A. and Cooper, B. H. (1995) *Physical Review Letters*, **75**, 1654-1657.
- Kim, C., Hofner, C. and Rabalais, J. W. (1997) *Surface Science*, **388**, L1085-L1091.
- Kim, Y. S., Jung, Y. J., Kang, W. Y. and Jung, K. H. (2002) *Bulletin of the Korean Chemical Society*, **23**, 189-194.
- Kimmel, G. A. and Cooper, B. H. (1993) *Physical Review B*, **48**, 12164-12177.
- Koenders, B. G., Kuik, G. J., Drabe, K. E. and Delange, C. A. (1988) *Chemical Physics Letters*, **147**, 310-314.
- Kokalj, A. and Causa, M. (1999) *Journal of Physics: Condensed Matter*, **11**, 7463-7480.
- Kolodney, E., Tsipinyuk, B., Bekkerman, A. and Budrevich, A. (1997) *Nuclear Instruments & Methods in Physics Research Section B- Beam Interactions with Materials and Atoms*, **125**, 170-184
- Kuipers, E. W., Vardi, A., Danon, A. and Amirav, A. (1991) *Physical Review Letters*, **66**, 116-119.
- Kurepa, M. V., Babic, D. S. and Belic, D. S. (1981) *Journal of Physics B-Atomic Molecular and Optical Physics*, **14**, 375-384.
- Lahaye, R. and Kang, H. (2001) *Surface Science*, **490**, 327-335.
- Lahaye, R., Stolte, S., Kleyn, A. W., Smith, R. J. and Holloway, S. (1994) *Surface Science*, **309**, 187-192.
- Lavery, A. C., Sosolik, C. E., Keller, C. A. and Cooper, B. H. (2000) *Physical Review B*, **61**, 2291-2301.
- LeRoy, R. J. (2001) University of Waterloo, Canada.
- Lide, D. R. (Ed.) (1999) *CRC Handbook of Chemistry and Physics*, CRC Press, New York.

- Lim, C., Tully, J. C., Amirav, A., Trevor, P. and Cardillo, M. J. (1987) *Journal of Chemical Physics*, **87**, 1808-1816.
- Los, J. and Geerlings, J. J. C. (1990) *Physics Reports-Review Section of Physics Letters*, **190**, 133-190.
- Maazouz, M., Maazouz, P. L. and Jacobs, D. C. (2002) *The Journal of Chemical Physics*, **117**, 10917-10920.
- Maazouz, M., Morris, J. R. and Jacobs, D. C. (2001) *Ion Imaging in Surface Scattering*, American Chemical Society, Washington, D.C.
- Martin, J. S., Greeley, J. N., Morris, J. R., Feranchak, B. T. and Jacobs, D. C. (1994) *Journal of Chemical Physics*, **100**, 6791-6812.
- Martin, J. S., Greeley, J. N., Morris, J. R. and Jacobs, D. C. (1992) *Journal of Chemical Physics*, **97**, 9476-9479.
- Martina, L. and Poltras, D. (2000) *Journal of Vacuum Science & Technology a- Vacuum Surfaces and Films*, **18**, 2619-2645.
- Mashkova, E. S. and Molchanov, V. A. (1985) *Medium-Energy Ion Reflection from Solids*, North-Holland, Amsterdam.
- Merino, J. and Marston, J. B. (1998) *Physical Review B*, **58**, 6982-6991.
- Morozov, V. A. and Meyer, F. W. (2001) *Physical Review Letters*, **86**, 736-739.
- Morris, J. R. (1996) In *Department of Chemistry and Biochemistry* University of Notre Dame, Notre Dame.
- Morris, J. R., Kim, G., Barstis, T. L. O., Mitra, R. and Jacobs, D. C. (1997a) *Journal of Chemical Physics*, **107**, 6448-6459.
- Morris, J. R., Kim, G., Barstis, T. L. O., Mitra, R., Quinteros, C. L. and Jacobs, D. C. (1997b) *Nuclear Instruments & Methods in Physics Research Section B- Beam Interactions with Materials and Atoms*, **125**, 185-193.
- Morris, M. R., Riederer, D. E., Winger, B. E., Cooks, R. G., Ast, T. and Chidsey, C. E. D. (1992) *International Journal of Mass Spectrometry and Ion Processes*, **122**, 181-217.
- Nakanishi, H., Kasai, H. and Okiji, A. (1991) *Surface Science*, **242**, 410.
- Nordlander, P. and Tully, J. C. (1990) *Physical Review B*, **42**, 5564-5578.

- Overbosch, E. G., Rasser, B., Tenner, A. D. and Los, J. (1980) *Surface Science*, **92**, 310-324.
- Potts, A. W. and Price, W. C. (1971) *Transactions of Faraday Society*, **46**, 1242.
- Qinyuan, W. and Hanley, L. (1993) *Journal of Physical Chemistry*, **97**, 2677.
- Reijnen, P. H. F., Vanslooten, U. and Kleyn, A. W. (1991) *Journal of Chemical Physics*, **94**, 695-703.
- Rettner, C. T. (1992) *Physical Review Letters*, **69**, 383-386.
- Rettner, C. T. (1994) *Journal of Chemical Physics*, **101**, 1529-1546..
- Rettner, C. T. and Auerbach, D. J. (1995) *Physical Review Letters*, **74**, 4551-4554.
- Rettner, C. T., Auerbach, D. J. and Lee, J. (1996) *Journal of Chemical Physics*, **105**, 10115-10122
- Roncin, P., Borisov, A. G., Khemliche, H., Momeni, A., Mertens, A. and Winter, H. (2002) *Physical Review Letters*, **89**, art. no.-043201.
- Roy, R. J. L., Macdonald, R. G. and Burns, G. (1976) *Journal of Chemical Physics*, **65**, 1485-1500.
- Schlienz, H., Beckendorf, M., Katter, U. J., Risse, T. and Freund, H. J. (1995) *Physical Review Letters*, **74**, 761-764.
- Schubert, S., Imke, U. and Heiland, W. (1989) *Surface Science*, **219**, L576-L582.
- Schultz, D. G. and Hanley, L. (1998) *Journal of Chemical Physics*, **109**, 10976-10983.
- Shao, H., Langreth, D. C. and Nordlander, P. (1994) *Low Energy Ion-Surface Interactions*, Wiley, New York.
- Silva, J., Borisov, A. G., Gauyacq, J. P., Nordlander, P., Teillet-Billy, D. and Wolfgang, J. (1999) *Nuclear Instruments & Methods in Physics Research Section B- Beam Interactions with Materials and Atoms*, **157**, 55-60.
- Silva, J., Wolfgang, J., Borisov, A. G., Gauyacq, J. P., Nordlander, P. and Teillet-Billy, D. (2002) *Surface Science*, **506**, 145-160.
- Sitz, G. O. (2002) *Reports on Progress in Physics*, **65**, 1165-1193.

- Smedley, J. E., Haugen, H. K. and Leone, S. R. (1987) *Journal of Chemical Physics*, **87**, 2700-2708.
- Smith, R., Beardmore, K., Grasmarti, A., Kirchner, R. and Webb, R. P. (1995) *Nuclear Instruments & Methods in Physics Research Section B- Beam Interactions with Materials and Atoms*, **102**, 211-217.
- Smith, R. and Webb, R. P. (1993) *Proceedings of the Royal Society of London Series a- Mathematical Physical and Engineering Sciences*, **441**, 495-499.
- Sosolik, C. E. and Cooper, B. H. (2001) *Nuclear Instruments & Methods in Physics Research Section B- Beam Interactions with Materials and Atoms*, **182**, 167-173.
- Sosolik, C. E., Hampton, J. R., Lavery, A. C., Cooper, B. H. and Marston, J. B. (2003) *Physical Review Letters*, **90**, art. no.-013201.
- Sulston, K. W. and Davison, S. G. (1992) *Surface Science*, **261**, 335-341.
- Sulston, K. W. and Goodman, F. O. (2000) *Journal of Chemical Physics*, **112**, 2486-2489.
- Tucek, J. C. and Champion, R. L. (1997) *Surface Science*, **382**, 137-146.
- Tully, J. C. (1980) *Journal of Chemical Physics*, **73**, 6333-6342.
- van Slooten, U., Andersson, D. R., Kleyn, A. W. and Gislason, E. A. (1992) *Surface Science*, **274**, 1-20.
- Wahnstrom, G., Lee, A. B. and Stromquist, J. (1996) *Journal of Chemical Physics*, **105**, 326-336.
- Walkup, R. E. and Avouris, P. (1989) *Physical Review B*, **39**, 5504-5507.
- WaveMetrics (1988-2000) Lake Oswego, OR.
- Weinberg, W. H. (1991) (Ed, Ashfold, M. N. R.) Royal Society of Chemistry, London, pp. 171.
- Wiley, M. C. and McLaren, I. H. (1955) *Review of Scientific Instruments*, **26**, 1150.
- Winter, H. (1996) *Journal of Physics: Condensed Matter*, **8**, 10149-10183.
- Winters, H. F. and Coburn, J. W. (1992) *Surface Science Reports*, **14**, 161-269.

- Yang, M. C., Hwang, C. H. and Kang, H. (1997) *Journal of Chemical Physics*, **107**, 2611-2618.
- Yang, M. C., Kim, C., Lee, H. W. and Kang, H. (1996) *Surface Science*, **358**, 595-601.
- Zangwill, A. (1988) *Physics at Surfaces*, Cambridge University Press, Cambridge.
- Ziegler, J. F., Biersack, J. P. and Littmark, U. (1985) *The Stopping and Range of Ions in Solids*, Pergamon Press, New York.